ලංකා විදුලිබල මණ්ඩලය
இலங்கை மின்சார சபை
CEYLON ELECTRICITY BOARD

R&D Journal

June 2020

Edited by:

Dr. A. J. Y. D. Manoj
(Devaka Jayawardana)
Research and Development
Ceylon Electricity Board
ajydm@yahoo.com, ee2rd.cs@ceb.lk

Navodana Kankanamge
New Kelani Bridge Project
Ceylon Electricity Board
navodanak@gmail.com

Economic Evaluation and Optimization of Reactive Power Flow of Existing CEB Transmission System

K.M.C.P Kulasekara
National System Control Centre
Ceylon Electricity Board
Colombo, Sri Lanka
prabuddha4@gmail.com

Devaka Jayawardana
Research and Development
Ceylon Electricity Board
Colombo, Sri Lanka
ajydm@yahoo.com

G.B. Alahendra
Transmission Planning
Ceylon Electricity Board
Colombo, Sri Lanka
gbalahendra@gmail.com

***Abstract*— In Ceylon Electricity Board, generating the majority of system-required reactive power (Q) from installed generators is a well-known practice. Since the majority of CEB generating stations are located in far-away places to the load centers, the generated Q should flow through the transmission system from those places to load centers for system voltage stability requirements. However, economic evaluation and optimization of this Q flow are imperative to be researched. Hence, in this study, NCP and OPTFLOW software modules have been used to model the present power system and for optimization. Power system-related data of the year 2017 has been used in model training and optimization.**

Simulated model optimization has identified that Ratmalana, Pannipitiya, Sri Jayewardenapura, Horana, and Dehiwala Grid Substations as major locations for new capacitor bank additions with capacities of 40, 30, 30, 20 and 15 MVAr, respectively. Loss calculations have shown that 9321.6 MWh of energy could be saved in the power system for the study year, provided above optimized reactive power support.

Keywords*— *economic dispatch, economic evaluation, optimization, power system, reactive power

I. INTRODUCTION

At present, the Sri Lankan power system has a total installed capacity of 4159 MW including non-conventional renewable energy power plants. It consists of 1364 MW of large hydro plants, 2115 MW of thermal plants, and 680 MW of non-conventional renewable power plants. Non-conventional renewable energy sources include 361 MW of mini-hydro power plants, 124 MW of wind power plants, 168 MW of solar power plants, and 27 MW of biomass power plants. The typical night peak demand is around 2500 MW and the day peak is around 2200 MW in the year of 2018. Allowed frequency deviation in Sri Lankan power system is specified as +/- 1% of 50 Hz in the Grid Code and at least 5% from the total system generation should be kept as system hot spinning reserve margin to deal with recurrent frequency changes. System frequency may rise to 52 Hz or fall up to 47 Hz during severe disturbance situations and under frequency situations can be managed through the operation of automatic under frequency load shedding scheme.

The present transmission network comprises of 220 kV and 132 kV voltage levels along with the length of 601 km of 220 kV lines and 2,261 km of 132 kV lines. This transmission network interconnects 29 number of power stations and 65 number of grid substations including major 220/132 kV coupling points such as Biyagama, Pannipitiya, Kotugoda, Kelanitissa, New Anuradhapura, New Chilaw and Rantambe. According to the grid code, +/- 5% voltage regulation is allowed for planning purposes, and +/- 10% voltage regulation is allowed for the operational purpose for both 220 kV and 132 kV voltage levels. The distribution network is having 33 kV and 11 kV voltage levels and +/- 2% voltage regulation is allowed according to the grid code. The careful balance of reactive power is needed for an adequate supply of active power through the network to maintain system voltage levels in an acceptable range and at the same time guarantee system operation security. In the transmission network, there are different types of equipment that can generate or absorb reactive power in a controlled manner. The generators can generate or absorb reactive power through the control of the terminal voltage level. The maximum reactive power generation and absorption capacities of hydro and thermal power plants have been represented in Table I.

The capacitor or reactor banks are cheaper and adequate for the cases when changing the need of reactive power requirement is slow or quasi-static. The available capacitor banks' locations in the present transmission system and installed capacities are depicted in Table II.

TABLE I. REACTIVE POWER GENERATION AND ABSORPTION CAPABILITIES

Power Plant	Maximum Reactive Generation	Maximum Reactive Absorption
Kothmale	120	-90
Upper Kothmale	80	0
Victoria	120	-60
Randenigala	50	-20
Rantambe	20	0
Ukuwela	20	0
Bowatenna	15	0
Canyon	10	0
New_laxapana	60	-30
Polpitiya	34	-6
Wimalasuren	10	0
Old laxapana	12	0
Samanalawewa	54	-20
Kukule	24	0
Lakvijaya	270	-180
Sapugaskanda A	12	8
Sapugaskanda B	16	4
Barge	12	4
KCCP	115	-10
Kel GT07	35	5
Kel Small GTs	25	0
Uthuru Janani	10	0
Sojitz	40	-5
WCP	120	-8
ACE Matara	6	0
ACE Embilipitiya	42	0
Asia power	*32*	*6*
Emergency power	10	0

TABLE II. LOCATIONS AND CAPACITIES OF AVAILABLE CAPACITOR BANKS

Connected Grid Substation	**Installed Capacity MVAr**
Ambalangoda	10
Ampara	30
Aniyakanda	10
Athurugiriya	10
Habarana	10
Katuayake	20
Kelaniya	20
Kiribathkumbura	20
Kotugoda	50
Kurunegala	10
Mathugama	20
New Galle	30
Pallekelle	20
Panadura	20
Puttalam	20
Thulhiriya	10
Total Installed Capacity	**310**

Synchronous condensers or static VAr compensators have been designed for the cases when a fast response of reactive support is needed, in the cases of contingencies or sudden load changes. In addition, controllable tap changers of transformers are important in overall voltage control as they can change network reactive power flow to adjust bus voltage levels.

Moreover, the high voltage transmission lines have an inherent characteristic of self-producing capacitive or inductive reactive power along the length of the transmission line. This is due to the distributed nature of the charging current caused by shunt capacitance due to the electrostatic field of the earth. The amount of reactive power that a transmission line provides to the system is related to the line voltage. The greater the voltage, the more MVAr will be supplied by the line. Furthermore, the transmission lines absorb reactive power in high load or when generation is far from the load centers. On the other hand, in light load, the same transmission lines generate reactive power and reactive absorption is needed to avoid the increase in voltage level.

II. MODELING THE EXISTING SYSTEM

A. Modeling Tool

NCP software module along with the OPTFLOW module have been used to model and simulate the present power system. NCP is a mixed-integer linear programming model designed to identify the optimum dispatch of an electrical system composed of hydro and thermal generation plants. NCP can be integrated with long term models (SDDP Model) through the use of future cost functions, target storage, or target generation constraints. NCP can be simulated for a horizon up to one month (744 hours), with 60, 30 or 15 minutes timesteps. It has a linearized DC power flow model with quadratic losses to represent the transmission network. It is fully integrated with the OPTFLOW Model, an optimum AC power flow model which calculates the reactive compensation requirements based on the NCP results.

OPTFLOW is an AC optimal power flow model that determines the optimal operation of generation and transmission system, representing the AC network constraints like bus voltage limits, reactive power limits, etc. in an integrated form. The OPTFLOW model is used for applications in optimal probabilistic system operation and transmission system planning. OPTFLOW is modeled as a nonlinear optimization problem whose constraints include Kirchoff´s laws, network operating limits, and constraints of the generation system. The objective function of OPTFLOW is the minimum injection of reactive power sources which helps to identify the need for reactive power injection to operate the system without violations. The optimal system operation determines the scheduling of thermal and hydro generation that minimizes expected operation costs. This optimization problem is complex because the AC power flow equations are nonlinear.

This is a mixed-integer nonlinear programming problem, which is achieved by iteratively solving in OPTFLOW for different reinforcement alternatives. The minimum and maximum voltage limits are operative limits of the network and they must be as close as possible to the real operation voltage level of the bus. After execution of OPTFLOW, all the voltage levels will be within the specified limits and it is guaranteed by construction in the Interior Point Method algorithm.

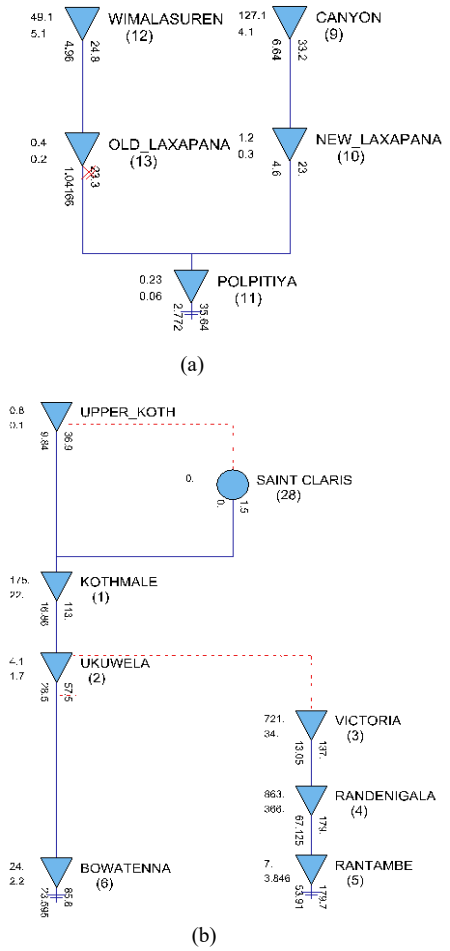

Fig. 1. Topological arrangements: (a) Laxapana copmlex and (b) Mahaweli complex.

.

B. Modeling the Hydro Power System

The Sri Lankan power system has mainly three hydropower complexes such as Laxapana complex, Mahaweli complex, and Samanala Complex. Based on the geographical and hydrological conditions, each complex has its generation constraints and water release requirements like drinking water, irrigation, and environmental releases, etc. The topological arrangements of Laxapana complex and Mahaweli complex have been illustrated in Fig.1(a) and Fig.1(b), respectively.

C. Modeling Thermal Power System

There are three types of costs involved with thermal plants which include operating cost, startup cost, and shut down cost. These costs are subjected to be varied from plant to plant depending on the use of fuel and type of power plant. It is possible to represent thermal consumption factors or specific consumptions (fuel units/MWh) varying from one to three segments, following the dispatched output of the unit as shown in Fig. 2. In this case, the operating cost of the thermal unit results in a linear function of separate segments. The startup costs of combined cycle power plants have been considered in three steps depending on the desynchronize time as hot, warm, and cold startups.

D. Modeling the Transmission System

The transmission network system consists of a set of busses and a set of circuits where the generators and demands are connected so that energy can be transferred between them. Total transmission network has been modeled in NCP from generator bus bars voltage levels to distribution bus bars voltage levels. Further, all transmission circuits have been assigned line resistance, reactance, susceptance, and load flow limit for the simulation of AC load flow. Moreover, all bus bars have been given latitude and longitude coordinates and resultant geographical view of the total transmission network along with power stations and grid substations is shown in Fig.3.

Losses in the transmission circuits vary with the square of the circuit flow. Thus, it is important to have a criterion to define the number of segments to be utilized for the linear approximation by parts, of the loss function of each circuit. The reason is, the greater the number of segments, the better is the linear approximation of the quadratic loss function, but the greater becomes the increase of the number of problem variables and it will consume more time to converge. Hence, when approximating the quadratic loss function with segments, it should be estimated so that the maximum error is minimized and variation of losses with circuit flow for five segments is shown in Fig. 4.

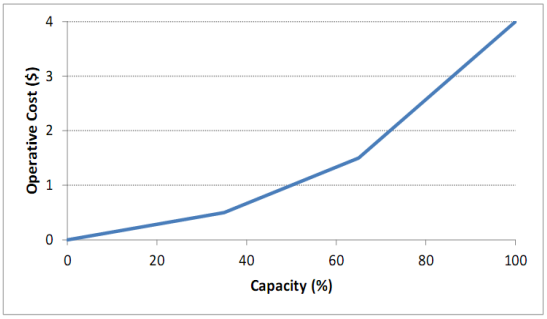

Fig. 2. Variation of operative cost with dispatched capacity.

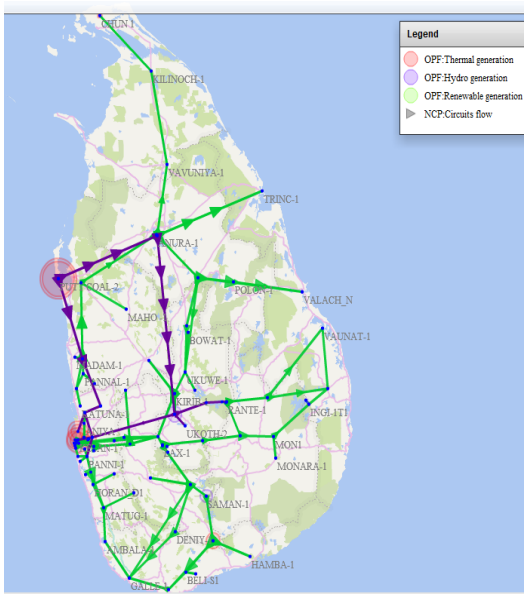

Fig. 3. Geographical representation of transmission network along with power stations and grid substations.

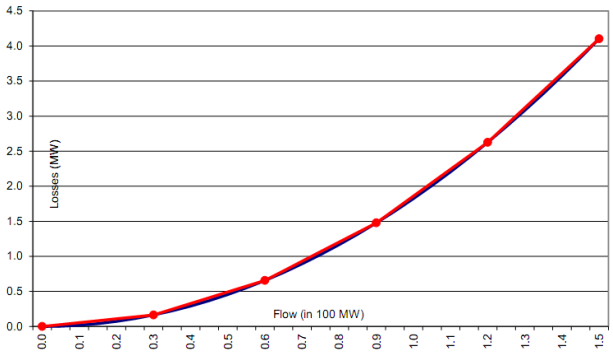

Fig. 4. Linear approximation of losses with circuit flow for five segments.

E. Input Parameters for Software Model

The grid wise demand data and power factor have been extracted from data files that were available at Energy Marketing Branch, CEB. The actual bus wise demand for the year 2017 was entered in 30-minute intervals and the power factor was calculated and entered in one-hour intervals. The minimum and maximum voltage limits were assigned as shown in Table III. The hydro-thermal coordination was done through the future cost function which was extracted from the SDDP model. Future cost functions have been generated month-wise from the SDDP model and used as a terminal function for the NCP model.

TABLE III. MINIMUM AND MAXIMUM VOLTAGE LIMITS

Voltage Level	Voltage Regulation
220 kV	0.95 p.u. to 1.05 p.u.
132 kV	0.95 p.u. to 1.05 p.u.
33 kV	0.98 p.u. to 1.02 p.u.
11 kV	0.98 p.u. to 1.02 p.u.

TABLE IV. INJECTION COSTS OF CAPACITOR BANKS

Voltage Level	Injection Cost
220 kV	1.167 $/MVArh
132 kV	0.680 $/MVArh
33 kV	0.175 $/MVArh

The minimum spinning reserve margin is considered as 5% of the total system generation and the maximum generation from a single unit is limited to 25 % of the total system generation as reliability constraints. The injection cost of the capacitor banks at 33 kV voltage level was calculated from the data at the Transmission and Generation Planning Branch, CEB, and the injection costs at 132 kV and 220 kV voltage levels were derived as given in Table IV, based on 33 kV level injection costs.

III. SIMULATION AND RESULTS

A. Study Scenarios

Four generation scenarios were identified based on the demand and weather pattern in Sri Lanka. Accordingly, four separate study cases were developed and simulated so that it can cover the whole year 2017. Further, all studies were carried out for three days and the results of the second day have been extracted for analysis and comparisons. The considered generation pattern and study period for an individual scenario are tabulated in Table V.

The months of February, March, and April were considered as dry months and the days from 15th to 19th March 2017 were considered for demand and power factor calculations. High system demand was recorded during this period due to high environmental temperature. NCP and OPTFLOW simulations were carried out and resulted hydro and thermal dispatch for a weekday along with losses are depicted in Fig. 5.

TABLE V. GENERATION SCENARIO ALONG WITH GENERATION PATTERN AND STUDY PERIOD

Scenario	Generation pattern	Study period
Case 01: **Dry condition**	High temperature/High Colombo demand, High solar, Low Mahaweli, Low Laxapana	15th – 19th March 2017
Case 02: **Wet condition**	High mini-hydro, High Mahaweli, High Laxapana	8th – 12th November 2017
Case 03: **Balance condition**	Balanced Hydro and thermal Mahaweli and thermal balance Laxapana and thermal balance	18th – 22nd January 2017 14th – 18th June 2017
Case 04: **High NCRE**	High wind and mini-hydro profiles	17th – 21st May 2017

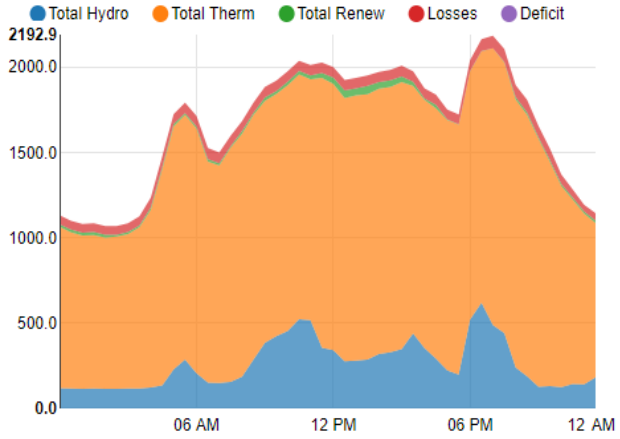

Fig. 5. Hydro and thermal dispatch to meet total system demand.

Accordingly, it can be seen that the thermal power plants have been used as baseload plants and most of the hydro plants have been dispatched only to meet the system peak demand.

The reactive power injections of existing capacitor banks over three days have been illustrated in Fig. 6. It can be observed that high reactive power injection during day time and partial or zero capacitive injection during the early morning hours of the day. Further, new reactive power additions were observed as shown Fig. 7, after the execution of OPTFLOW and new injections were limited only to day time and night peak hours where high reactive power consumption exists and due to additional cost associate with new additions.

B. Sensitivity Analysis

The simulations were carried out repeatedly for different capacitive power injection costs to identify the importance of injection cost to decide the location and dispatch amount of reactive power. Accordingly, it can be observed that new reactive injections of some GSSs were started from 8:30 hrs. and remains up to 20:00 hrs. while others are limited only to day time operation.

Then, for the sensitivity analysis and the comparisons, the major reactive injection locations of Rathmalana, Pannipitiya, Sri Jayawardhanapura, Horana, and Dehiwala GSSs were filtered out. Accordingly, the reactive power dispatch of the aforementioned GSSs for the injection cost of 0.15, 0.175, 0.2, 0.25, and 0.3 $/MVArh have been evaluated. The change of reactive power dispatch with the change of injection cost at Pannipitiya GSS has been illustrated in Fig. 8 along with a zoom-in view at day peak hours.

Accordingly, it can be observed that the reactive power dispatch amount has been reduced slightly with the increase of reactive power injection cost. Further, the maximum reactive power injection difference has been evaluated for aforesaid GSSs and it was observed that 1.47, 1.75, 1.93, 1.35 and 1.67 MVAr at Rathmalana, Pannipitiya, Sri Jayawardhanapura, Horana, and Dehiwala GSSs respectively for the injection cost of 0.15 $/MVAr and 0.3 $/MVAr. Thus, it was not observed a significant change in reactive power addition with the increase of reactive power injection cost, and accordingly, it was decided to use 0.175 $/MVArh for the simulations as 33 kV reactive power injection cost.

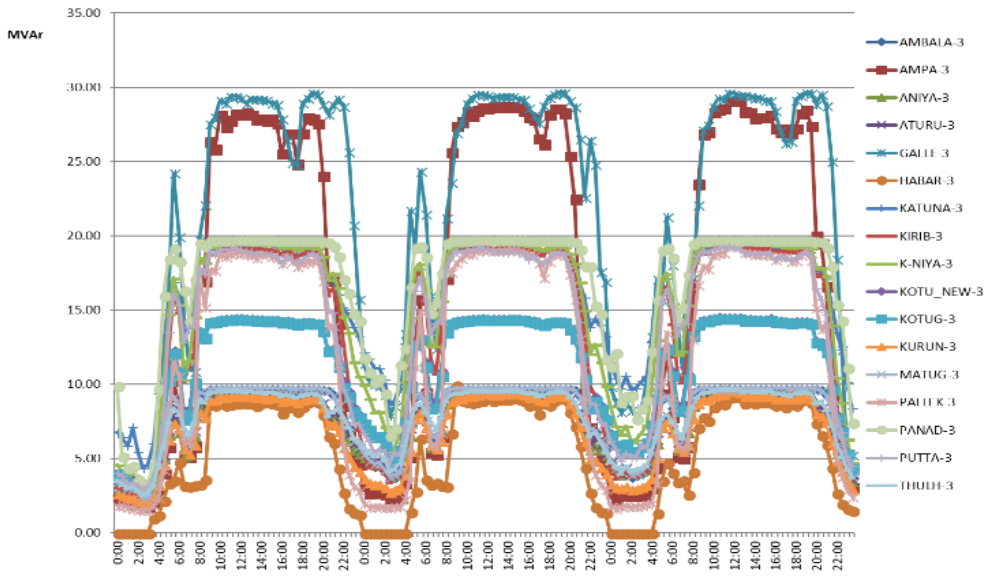

Fig. 6. Reactive power injection from existing capacitor banks.

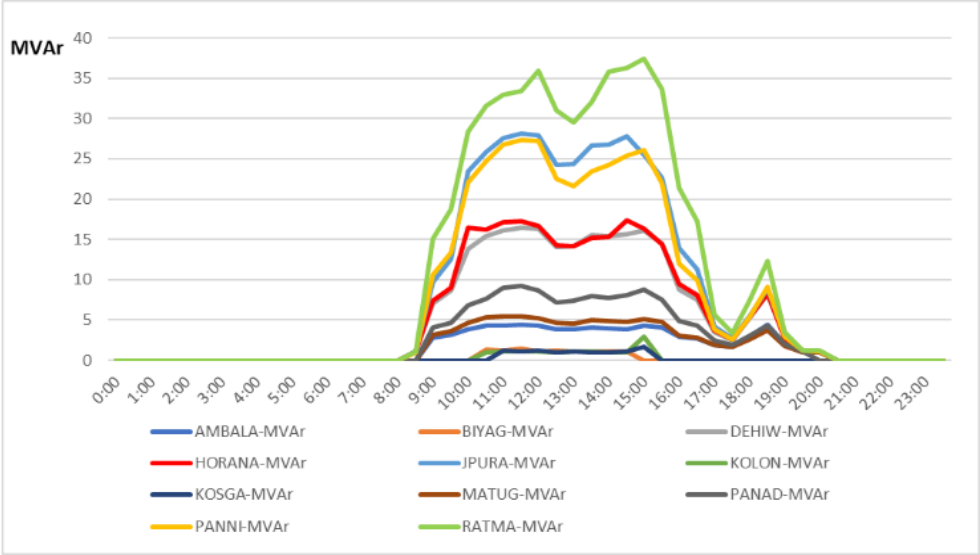

Fig. 7. New reactive power injection vs time.

C. *Comparison of the Behavior of the System with and without Reactive Power Addition*

To compare the behavior of the system, another case was developed by allowing OPTFLOW to drawdown 220, 132, and 33 kV bus bar voltages by violating grid code requirements so that new reactive additions become zero and compared the two cases to observe the difference of voltages and losses. As mentioned earlier, simulations were carried out for a 72-hour load profile, and the results of the second-day load profile have been extracted for comparisons.

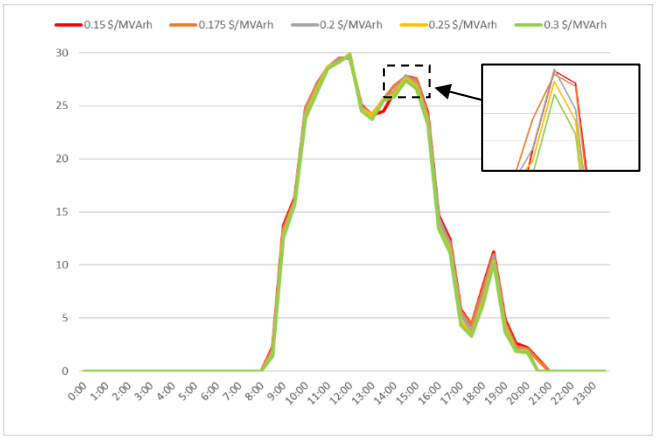

Fig. 8. Reactive power dispatch with a change of injection cost at Pannipitiya GSS.

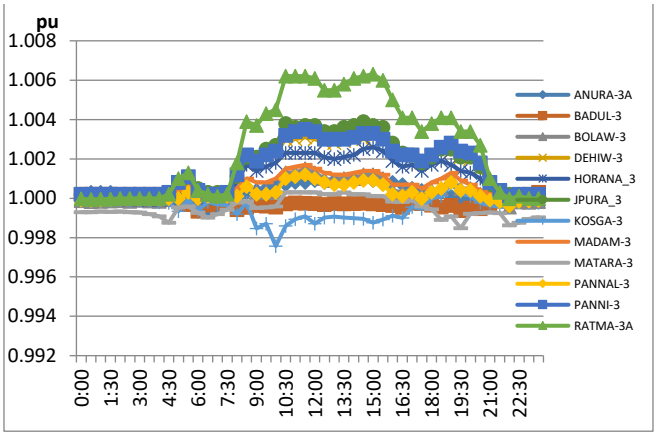

Fig. 9. Voltages of 33-kV bus bar after new reactive power additions.

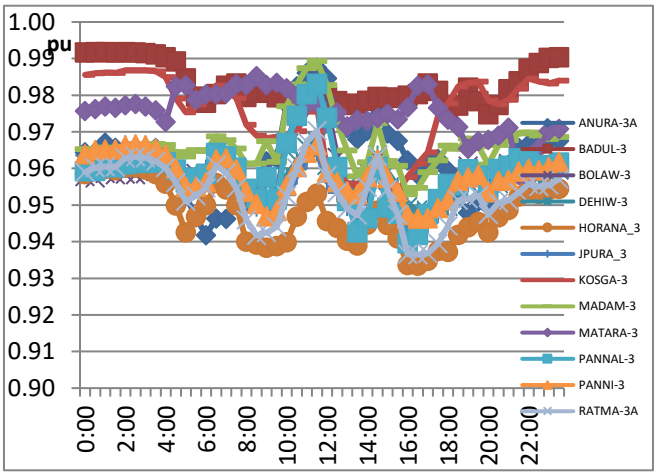

Fig. 10. Voltages of 33-kV bus bar without new reactive power additions.

Accordingly, 33 kV bus bar voltages were compared with and without new reactive additions, and Fig. 9 and Fig. 10 demonstrate the voltage variation throughout the 24 hours load profile with and without reactive power additions, respectively. According to Fig. 9, it can be observed that with the new reactive power additions, most of the 33 kV bus bar voltages were maintain around 1.0 p. u and minimum voltage drop recorded at Kosgama bus bar with 0.997 p. u which is well above the grid code requirements. However, Fig. 10 shows that the average 33-kV bus bar voltages were maintained around 0.97 p. u without new reactive additions and minimum voltage was recorded at Horana 33 kV bus bar to 0.933 p. u while violating system grid code requirements up to a greater extent.

Some 33 kV bus bar voltages have been maintained slightly above 1.0 p. u during day time and night peak hours. Rathmalana, Pannipitiya, Dahiwala, Horana, and Sri Jayewardhanapura GSSs were some of them and it was identified that slight voltage rises due to the new capacitive power injection during day time and night peak hours.

Further, 132 kV and 220 kV voltage levels have been analyzed for both cases and Fig. 11 and Fig. 12 illustrates the 132 kV voltage variation over the 24-hour schedule with and without new reactive additions. As depicted in Fig. 11, a minimum voltage level of 0.95 p. u at 132 kV side was recorded in Matara GSS at night peak hours.

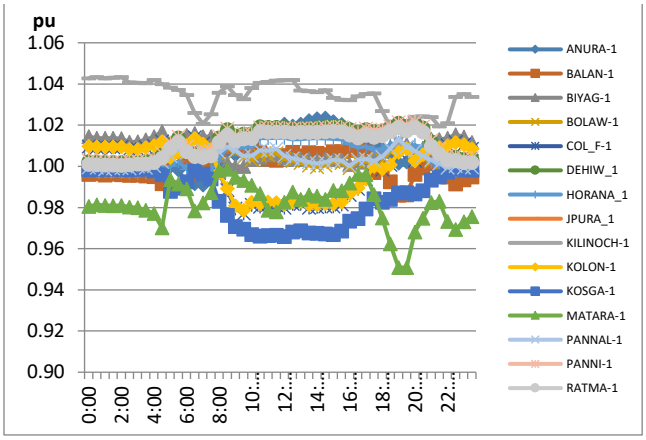

Fig. 11. Voltages of 132-kV bus bar after new reactive power additions.

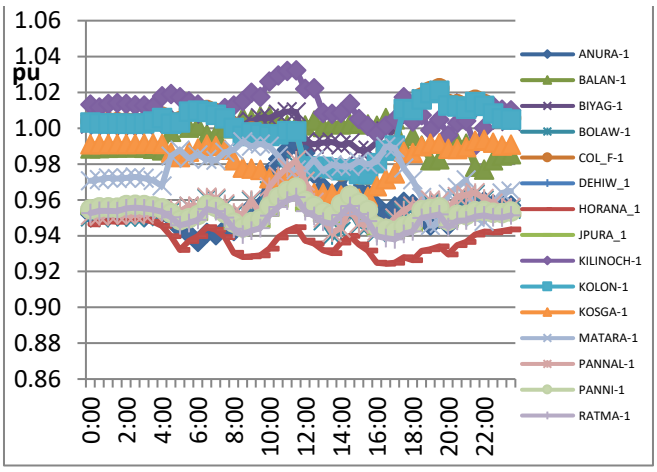

Fig. 12. Voltages of 132-kV bus bar without new reactive power additions.

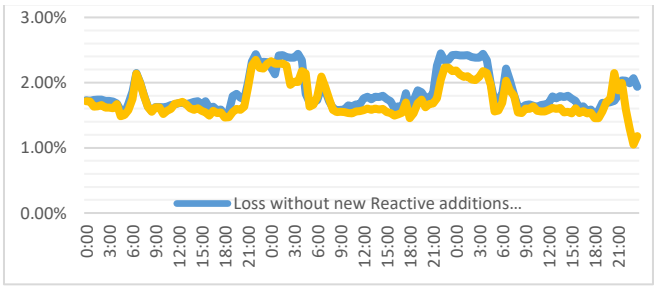

Fig. 13. Variation of losses with time.

Further, an average 132 kV voltage has maintained around 1.0 p. u after new reactive additions. However, according to Fig. 12, the average 132 kV bus bar voltage has dropped and maintained around 0.97 p. u and minimum voltage has dropped up to 0.92 p. u in Horana GSS during day time hours.

Further, 220 kV bus bar voltage levels were analyzed and compared for both cases. However, it was not observed a significant voltage difference in 220 kV level with and without new reactive power additions. Moreover, loss analysis was carried out for all three days of simulation profile and comparison of loss profiles before and after new reactive additions were shown in Fig. 13. The diagram represents the percentage of losses with respect to total system generation over the 72-hour load profile. Then, energy-saving was calculated as illustrated in Fig. 14, for the second 24 hours period and it was observed that 46.11 MWh of energy can be

saved per day with the addition of proposed new capacitor banks.

The months of September, October, and November have been considered as wet duration and the days from 8th to 12th November 2017 were considered for the demand and power factor calculations. During this period, comparatively lower demand is recorded due to low environmental temperatures. The average inflow of November and the future cost function of November 2017 has been used as the hydrological conditions for the NCP model.

The energy-saving was calculated as illustrated in Fig. 15, for the second 24 hours period and it was observed that 29.35 MWh of energy can be saved per day with the addition of new capacitor banks from optimization. With the behavior of the two monsoons in Sri Lanka, two separate periods have been identified for the simulation of the balance generation scenario. The months of December and January considered for the balance condition where high reservoir storages present with lower water value at the Mahaweli system. Thus, days from 18th to 22nd January 2017 were considered for demand and power factor calculations. The months of June and July have been considered as the second time slot where the Laxapana complex having a high reservoir level with lower water value. Accordingly, the demand and power factor calculations were done for the days from 14th to 18th June 2017.

The energy-saving was calculated separately for both stages as illustrated in Fig. 16 and Fig. 17. It was observed that 40.02 MWh of energy can be saved per day for December, January, and 31.21 MWh of energy can be saved per day for June and July with the addition of proposed new capacitor banks.

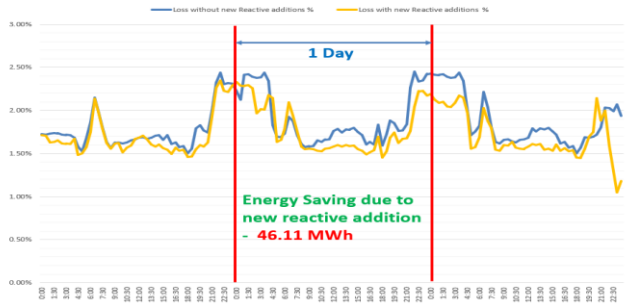

Fig. 14. Variation of losses and energy saving for the dry scenario.

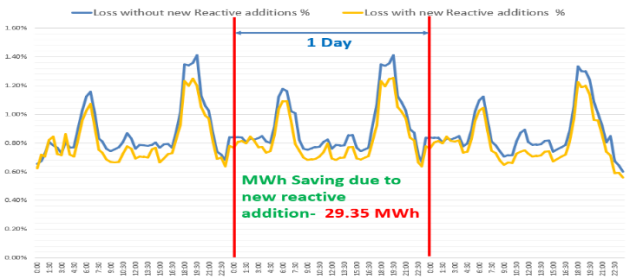

Fig. 15. Variation of losses and energy saving for the wet scenario.

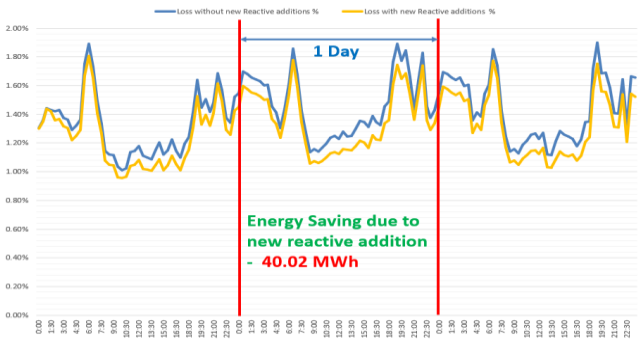

Fig. 16. Variation of losses and energy saving for Mahaweli high scenario.

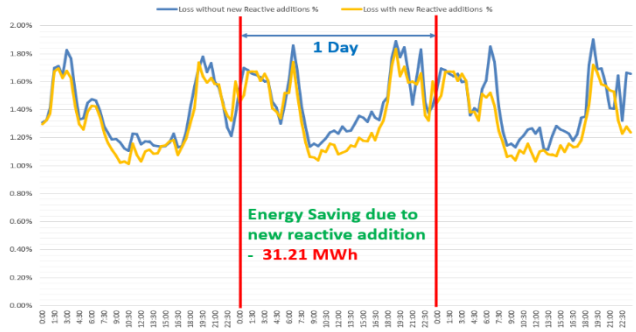

Fig. 17. Variation of losses and energy saving for Laxapana high scenario.

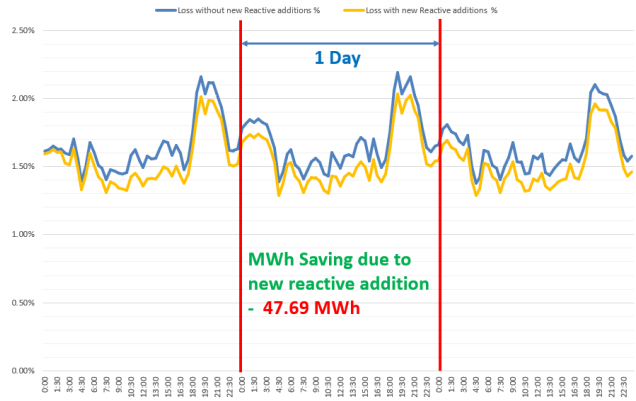

Fig. 18. Variation of losses and energy saving for high NCRE scenario.

By considering the high Wind, Mini Hydro and Solar profiles, months of May and August have been considered for the simulation of high NCRE generation scenario. Thus, days from 17th to 21st May 2017 were considered for demand and power factor calculations. The energy-saving was calculated as illustrated in Fig. 18 and it was observed that 47.69 MWh of energy can be saved per day for high NCRE condition with the addition of proposed new capacitor banks.

All aforementioned simulations were carried out so that they can represent the behavior of generation and transmission system for the whole year. The amount of new capacitive power dispatch of highly injected locations was summarized in Table VI for all the aforementioned scenarios. Accordingly, high reactive power injections were observed during dry and high NCRE scenarios while lowest reactive power injection was observed during the wet season. The

highest reactive power injection for all scenarios was recorded from Rathmalana GSS as given Table VI.

According to the simulations, new capacitor additions were not observed for Sundays or holiday load profiles. However, for the Saturday load profiles, energy saving was calculated as 0.7 times from the respective weekday load profile. Then, total energy saving was calculated as shown in Table VII and it was found that 9321.60 MWh of energy can be saved yearly with the addition of new capacitor banks.

TABLE VI. MAXIMUM AMOUNT OF CAPACITIVE POWER INJECTION FOR DIFFERENT SCENARIOS

Study Scenario	Maximum reactive power injection/MVAr				
	Dehiwala	Horana	Sri J'pura	Pannipitiya	Rathmalana
Dry Scenario	17.37	19.94	29.94	29.59	38.84
Wet Scenario	7.05	7.66	9.99	7.82	17.94
Balance Scenario-Mahaweli major	14.80	18.05	25.17	21.74	37.01
Balance Scenario-Laxapana major	14.87	16.63	23.61	20.68	35.40
High NCRE Scenario	20.07	22.43	32.27	30.71	46.11

TABLE VII. TOTAL ENERGY SAVING CALCULATION AFTER NEW REACTIVE POWER ADDITIONS

Study Scenario	Energy Saving/ (MWh/Day)	No. of Weekdays	No. of Saturdays	No. of Sundays/Holi Days	Total Energy Saving/MWh
Dry Scenario	46.11	60	12	19	**2775.00**
Wet Scenario	29.35	60	13	18	**1770.10**
Balance Scenario-Mahaweli major	40.04	40	9	13	**1607.90**
Balance Scenario-Laxapana major	31.21	40	9	11	**1254.70**
High NCRE Scenario	47.69	40	9	12	**1913.90**
Total annual energy saving					**9321.60**

IV. CONCLUSION

The comprehensive AC load flow study was carried out using NCP and OPTFLOW software models for the economic evaluation and optimization of reactive power flow of the existing CEB transmission system. The NCP software model was used to identify the optimum dispatch of the electrical system while OPTFLOW model was employed to calculate the reactive compensation requirement based on the NCP results, with respect to the voltage tolerances and all available resources of reactive supports such as capacitors/reactors banks, flexibility in adjusting tap of transformers and the terminal voltage of generators.

Following the modeling of the complete power system in NCP, AC load flow simulations were carried out for the demand data in 30 minutes interval for the year 2017. Four significant study cases were identified as Dry scenario, Wet scenario, Balance scenario, and high NCRE scenario so that they can be represented the major variations of weather and demand profiles of the whole year. Accordingly, new reactive power additions were identified other than the existing capacitive power injections for all scenarios with different dispatches. In conclusion, according to the OPTFLOW model, Rathmalana, Pannipitiya, Sri Jayawardhanapura, Horana, and Dehiwala GSSs were identified as major locations for new capacitor bank additions with the capacities of 40,30,30,20 and 15 MVAr respectively.

Further, from the loss analysis for the aforementioned scenarios, 9321.60 MWh of energy is determined for the simulated year with the addition of new capacitor banks as recommended by the OPTFLOW model. Thus, losses can be minimized with the addition of new capacitor banks especially at the designated locations of the present power system.

ACKNOWLEDGMENT

The authors would like to thank Mr. G. J. Aluthge, Deputy General Manager (Asset Management Thermal Electrical), Ceylon Electricity Board for his intellectual support as the supervisor of the study.

Voltage Impact of Roof-Top Solar Photo-Voltaic Systems on Low Voltage Network and Measures of Mitigation

K. G. R. F. Comester
Research and Development
Ceylon Electricity Board
Colombo, Sri Lanka
dgmrd@ceb.lk

D. D. K. G. Sandasiri
Planning and Development
Distribution Division -04
Ceylon Electricity Board
Colombo, Sri Lanka
kasun.sandasiri@ceb.lk

G. A. I. Mihindukulasuriya
Research and Development
Ceylon Electricity Board
Colombo, Sri Lanka
asirimihindu@gmail.com

K. P. J. P. Prematilake
Planning and Development
Distribution Division-03
Ceylon Electricity Board
Colombo, Sri Lanka
prabath.eng@gmail.com

Ruwani P. Wijesinghe
Energy Management
Western Province South-II
Ceylon Electricity Board
Colombo, Sri Lanka
ruwanipj@yahoo.com

K. Ratneswaran
Planning and Development
Distribution Division -02
Ceylon Electricity Board
Colombo, Sri Lanka
ratneswk@yahoo.com

U. G. J. K. Gamlath
Planning and Development
Distribution Division -01
Ceylon Electricity Board
Colombo, Sri Lanka
jayankagamlath@gmail.com

***Abstract*— Ceylon Electricity Board (CEB) Low Voltage (LV) distribution system is designed and operates on unidirectional power flow from generation to load. Nevertheless, with the advent of distributed generation, consumers are becoming prosumers, and the unidirectional power flow becomes bidirectional at different segments of the LV network. The distributed generation, especially solar PV generation, is a norm in power systems at present. Among the power quality issues creating owing to solar PV distributed generation in the LV network, it was identified that the voltage rise is the predominant factor impinging on the LV network adversely. In this research, the distribution transformers, which were penetrated significantly high in solar roof-top at the time of study conducted, were tested at four geographical locations. All electrical parameters at the transformers at the feeder ends were measured using external analyzers and at the solar PV generation points along the feeder were measured using existing data captures at the inverters. The analysis was made using the measured data, literature reviews, and Monte Carlo simulation technique. The outcome of this research is currently being utilized to determine the hosting capacity in CEB's LV network with current design and operation conditions and to understand how this limit can be increased.**

Keywords*— *hosting capacity, LV network, Monte Carlo simulation technique, roof-top solar PV, voltage rise

I. Introduction

Solar photovoltaic (PV) is one of the fastest developing renewable energy systems in Sri Lanka. Driven by governmental subsidies, technological development, and availability of net metering, net accounting, and net plus schemes, Sri Lanka has seen a fast expansion of roof-top solar PV in the last ten years. Out of them, a large number of roof-top solar PV systems are integrated at Low Voltage (LV) distribution system.

The LV integrated roof-top solar PV systems bring various operational challenges to the LV electricity distribution network. These challenges were researched in depth in this study to determine major influencing factors for the solar PV hosting capacity in CEB's LV network and to understand how this limit can be increased.

Scope of this research is as follows,

- Literature review on the impact of roof-top solar PV on LV Network Power Quality.
- Analysis of a sample LV schemes with Solar PV customers.
- Analysis of simplified radial LV Network with different Solar PV configuration using the Monte Carlo simulation technique.
- PV penetration limits in LV networks and propose other mitigation measures.

II. Literature Review

According to a large number of studies, over-voltage, harmonics, high losses, phase imbalance, islanding, power fluctuations, DC injection, frequency variations, and flicker can be varied due to the integration of distributed solar PVs [1]. However, in most of these studies, it has been concluded the voltage rise at the end of the feeders was the only power quality parameter that was significantly affected. For example, in a study conducted in 3 different countries of Europe with four different LV grid-connected roof-top PV systems in urban areas, it was concluded that the voltage rise

was the only power quality parameter (Under EN 50160) that was severely affected [2].

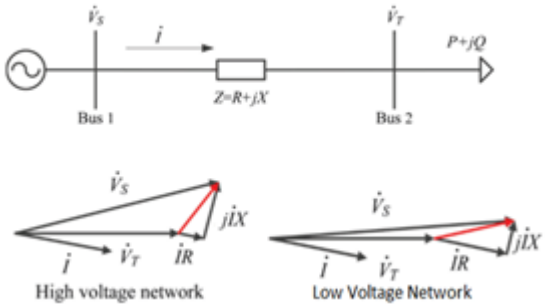

Fig. 1. Comparing the voltage drop characteristics at HV transmission and LV grid due to X/R ratios.

It can be showed that over-voltage generally occurs at peak PV generation hours with little or no load on LV feeders, mainly for two reasons: power flow reversal and reactive power disturbance in the circuit.

A. Theory of Voltage Rise

When there is reverse power flow, the high resistivity of residential LV networks compared to their typical reactance makes the voltage rise higher in the LV network than the high voltage (HV) transmission system. For instance, in a simple network, as shown in Fig. 1, neglecting the charging effect of the line, in the HV system, the magnitude of the resistance is much smaller than the reactance, whereas, in LV networks, it is the opposite situation.

From Fig. 1, the equation for the voltage drop across the line from Bus 1 to Bus 2 can be derived as follows.

$$\Delta V = I^*(R+jX) \quad (1)$$

$$\Delta V = ((P+jQ)/V_T)^*.(R+jX) \quad (2)$$

$$\Delta V = ((PR+QX)/V_T) + j((PX-QR)/V_T) \quad (3)$$

For High Voltage (HV) systems, since high X/R ratio, (3) for voltage drop can be simplified by ignoring the resistance effect as below in (4) & (5).

$$\Delta V = QX/V_T + j(PX/V_T) \quad (4)$$

$$\Delta V \approx QX/V_T \quad (5)$$

In contrast, in LV systems, since the X/R ratio is lower, the effect of resistance is no longer negatable, and assumptions taken for HV systems are no longer valid. Then, (3) for voltage drop can be simplified by ignoring the imaginary part as below in (6).

$$\Delta V = (PR + QX)/V_T \quad (6)$$

If a solar PV is connected at bus 2 in Fig. 1, Fig. 1 can be redrawn as Fig. 2, and V_T can be considered as V_{PCC}. Then, (6) can be rewritten as (7).

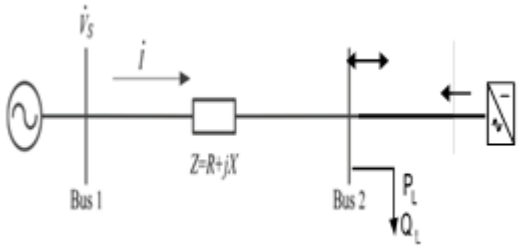

Fig. 2. Modified LV network with PV inverter.

$$V_{PCC} = V_S + (R(P_G - P_L) + X(Q_G + Q_c - Q_L))/V_{PCC} \quad (7)$$

For a residential roof-top Solar PV installation, Q_L & Q_c can be neglected, and Q_G=0 since the inverter is working at unity power factor. Then, from (7), under a light load condition, where P_L is small, it can be shown that the PCC Voltage will rise and can even exceed the grid code limitation as inverter injects more and more power into the system ($P_G >> P_L$).

From (7), it can be shown that voltage rise can be reduced either by increasing P_L, active power load, or through making Q_G <0 by operating inverter at negative power factor.

B. Voltage Rise PV Penetration Limits in Low Voltage Networks

In recent years, a reasonable number of studies have been published addressing the LV network voltage issue. However, the results from such studies were network-dependent and difficult to generalize and apply for CEB network mainly because the following factors played a leading role in these investigations.

- Network Topology.
- Types of Network components.
- Climatic conditions & solar irradiance level.
- Load profiles & load concentration along with feeders.
- Feeder lengths & types and sizes of conductors.
- Voltage Regulations in the Utility. (Example: ±10% in Europe, ± 5 % & ± 6 %)

As per the research paper in the reference [3], in almost every study done to find the PV penetration limit in LV networks, only limiting factor for determining the PV penetration limit was voltage. And in most of them, the PV penetration limit was found by simulation modeling techniques.

C. Definitions

In the literature, there is no straightforward definition for the solar PV penetration limit, which is widely agreed upon.

Therefore, in this study, roof-top Solar PV penetration is defined in a straight forward way as follows,

TABLE I. LIST OF MEASUREMENT STANDARDS FOLLOWED FOR FIELD MEASUREMENTS

PQ Parameter	**Measurement Standard /Allowed limit**
Line Voltage (V)	IEC 61000-4-30 class A / ±6% of the nominal voltage
Voltage THD (%)	IEC 61000-4-7 sub-group method /5% as per CEB manual
TDD (%)	IEC 61000-4-7 sub-group/ 5% as per CEB manual
Flicker (long term)	IEC 61000-4-15/ 1.0
Flicker (Short term)	IEC 61000-4-15/ 0.8

$$\text{PV penetration w.r.t Feeder} = \text{Installed PV inverter Peak Capacity (kWp) for a single feeder} \quad (8)$$

In this study, hosting capacity is defined as the maximum installed capacity of solar PV systems which is allowed to connect to the LV Feeder without causing voltage rise above 6 % of nominal voltage (230 V) at any point in the feeder.

D. Mitigation Measures

The following are some mitigation measures for voltage rise issues found in the literature.

- Introducing active & reactive power controlling algorithms to grid-tie inverters [4].
- Varying the scheduled changes to the distribution transformer tap [5].
- Using electronic on load Tap-changer (OLTC) equipped transformer (100 % increase in penetration level) [6].
- Using Battery Storage System (BSS) for houses [7].
- Introduce PV hosting capacity limits in LV networks.
- Limit individual PV inverter capacity by the distance from the transformer.
- Limit single-phase PV inverter capacity.

III. RESEARCH METHODOLOGY

A. Basic Methodology

Following research methodology was adopted to move forward the Solar PV integration study;

- Discussion with the Provincial / Area Engineers to identify the Solar PV integration issues.
- Literature review to study the present CEB's standards / International practices by other utilities for similar Solar PV integration issues /International Institutions.
- Data Collection & field measurement for the selected sample schemes under study.
- Model a feeder of one of the sample schemes with the Solar PV using power system modeling software.
- Analyze, calculate, and find out the under-voltage / over-voltage issues, and harmonic at different parts of the distribution network.
- Verify the data with the real field measurement. Record the findings.
- Recommendation for the Short term and long-term implementation.

B. Measurement Standards for Solar PV Integration in CEB's Distribution System

All the measurement standards followed for taking field measurements in this study, along with the allowed limit selected for each power quality parameter, are listed in Table I.

TABLE II. LIST OF SAMPLE LV SCHEMES SELECTED FOR THE STUDY

Location of the Case Study	**SIN**	**Research Problem & Observations**
Jayanthipura (2017)	T177	Analyzed the impact of Solar PV on harmonic level and other Power quality parameters Found that the impact of solar PV on the feeder voltage profile is significant. Studied how measuring interval will impact the voltage readings.
Diyawanna Gardens (2018)	TL10 9	Analyzed in detailed how Solar PV impact on feeder voltage profile. (Specially Voltage Rise issue) Transformer Capacity: 160 kVA Solar Penetration 71 kWp
Dehiwala (2018)	M027	Analyzed in detailed how Solar PV impact on feeder voltage profile. (Specially Voltage Rise issue) Transformer Capacity: 400 kVA Solar Penetration 90.2 kWp Recorded data were used for model validation.
Dinujayagama (2018)	R 082	Customers complained about lower energy generation from their roof-top solar PV than their expected monthly energy production. Transformer Capacity: 160 kVA Solar Penetration 60 kWp

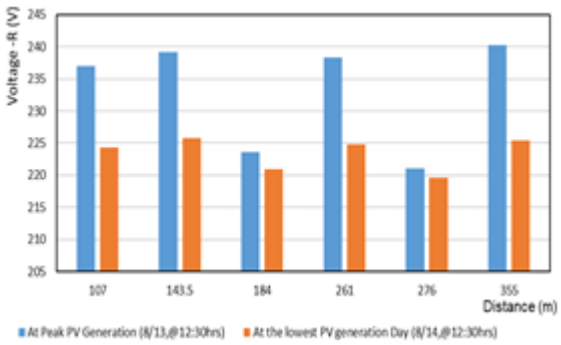

Fig. 3. Comparison of voltage profiles along the feeder in R-phase between the days of peak PV and lowest PV generation.

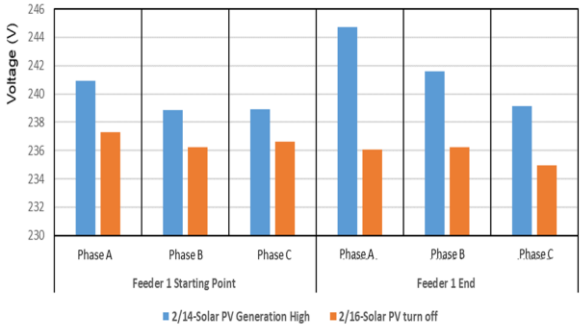

Fig. 4. Comparison feeder 1 starting point and feeder 1 endpoint voltages.

IV. Analysis of a Sample of LV Schemes with Solar PV Customers

All the sample LV schemes selected for this study, along with their research problems & significant observations are listed in Table II. In all of the listed case studies, during peak PV generation hours, voltage rise was observed at the point of common coupling between roof-top solar PV and LV network.

A. Observations of the Sample LV Scheme with Solar PV Customers (Jayanthipura T177)

Some significant observations made in the LV feeders of T177 Transformer in Jayanthipura are shown in Fig. 3. The voltages recorded along with R-phase of a feeder at the same time on the peak PV generation day and the lowest PV generation day are shown in Fig. 3. From this figure, it was observed that all voltages recorded along the feeder on the peak PV generation day were higher than the recorded voltages on the lowest PV generation day. Therefore, it is evident that power injection from the roof-top Solar PV system has a definite impact on the feeder voltage rise.

B. Observations of the Sample LV Scheme with Solar PV Customers (Dehiwala M027)

From Fig. 4, it was observed that voltages recorded at the same time at the feeder starting point and Feeder end on the peak PV generation day were higher than the voltages recorded at the same points on the day when Solar PVs were turned off. Therefore, from this figure also, it is evident that power injection from the roof-top Solar PV system has a definite impact on the feeder voltage rise, especially at the feeder end.

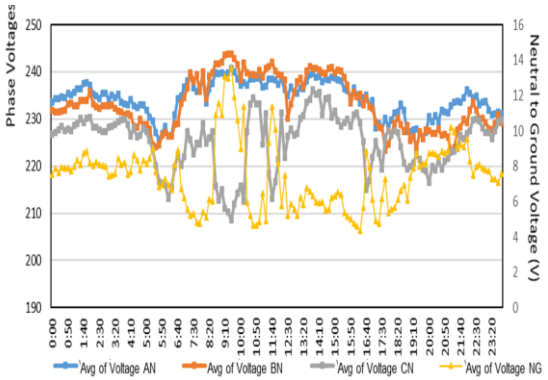

Fig. 5. Variation of the voltages of feeder 1 at mid-point on a peak PV generation day.

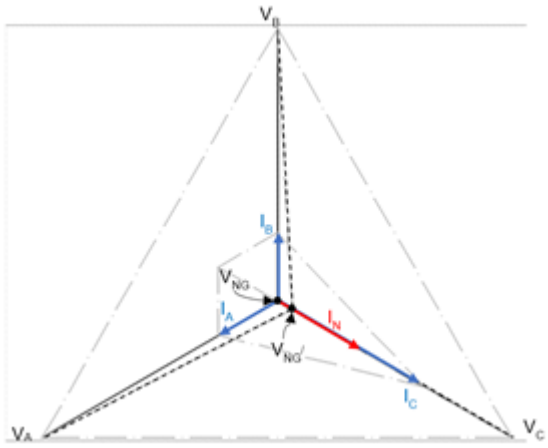

Fig. 6. The phasor diagram illustrates the inverse relationship between Phase C voltage and the natural to ground voltage.

C. Observations of the Sample LV Scheme with Solar PV Customers (Dinujayagama R082)

From Fig. 5, it was observed that there were voltage rises in phase A & phase B at feeder mid-point on a peak PV generation. It was also observed at this point that as neutral to ground voltage went above 8V, the voltage of phase C drastically came down to 208 V. The way how this happens can be explained by a three-phase phasor diagram as shown in Fig. 6.

D. Observations of the Sample LV Scheme with Solar PV Customers (Diyawanna Gardens TL109)

From Fig. 7, it was observed that the common coupling voltage of one phase had exceeded the grid code limitation (243.8 V) when the roof-top Solar PV power generation was high during the daytime. In these cases, it was found that inverter cut off voltage level had been set to 253 V (10 %). This is a clear violation of the CEB grid code. Usually, this inverter voltage cut-off setting is checked during the grid acceptance test. Therefore, it can be assumed that the PV supplier may have later changed this setting to a higher level after receiving customer complaints about frequent inverter tripping.

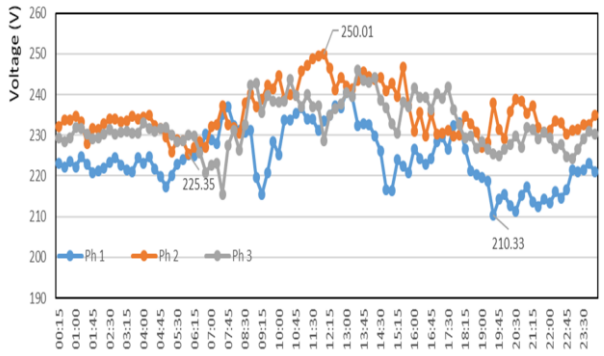

Fig. 7. Variation of common coupling voltages at F1-6 on the peak PV generation day.

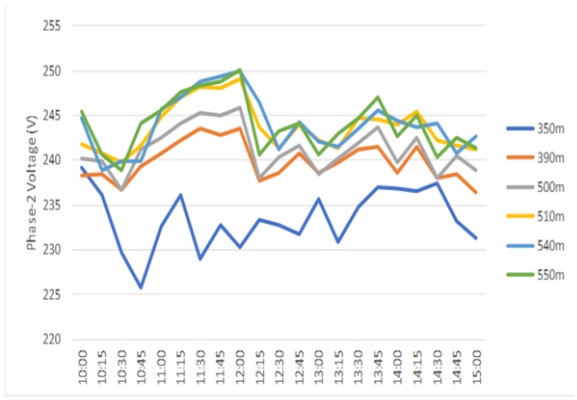

Fig. 8. Effects of voltage on feeder length.

In discussion with the provincial / area engineers, it was found that frequent inverter tripping due to voltage rise is a prevalent issue reported by customers in Jayawardenapura Area. From Fig. 8, it is shown how voltage varies with time at different distances from the transformer when the roof-top Solar PV power generation is high during the daytime. According to Fig. 8, it is evident that further away from the transformer, higher will be the voltage rise due to the reverse power flow of solar PV.

E. Summary of Observations

All significant observations of these 4 case studies can be summarised as follows.

- Impact of Solar PV on Voltage THD (%) and TDD (%) are low.
- Impact of Solar PV on flicker is negligible.
- Highest Voltage THD (%) values were recorded during Morning peak and Night Peak.
- As the PV penetration goes up, the voltage rise issue comes first before any other Power Quality issue.
- Voltage Rise is high when Solar PV power generation is high, and they were located far from the substation.
- Power injection from roof-top Solar PV impacts the voltage rise at the common coupling point.
- Voltage measurement can vary depending on the averaging interval used for recording.
- The voltage could even exceed the grid code limitation (243.8 V) due to roof-top Solar PV power generation.
- PV suppliers tend to change the inverter voltage cut-off level to a higher level (typically to 253 V) after receiving customer complaints about frequent inverter tripping which inevitably causes the common-coupling voltage to exceed the grid code limitation.
- PV inverters can even trip due to under-voltage conditions.

V. Simulation Modelling

In this research, OpenDSS Software was used to model voltage rise phenomena in LV networks with high PV penetration.

A. Input Parameters & Assumptions Applied in Modelling LV Networks

The following assumptions were made when these power system models were developed in OpenDSS software.

- All PV installations on the LV network are subject to the same irradiance variation.
- Generators have a constant power output vs voltage variation.
- The network can be simulated as sinusoidal 50 Hz with no harmonics.
- A constant power factor was assumed for generators, typically close to unity.
- The distribution transformer is a constant voltage source.
- Service cables were omitted from the model.
- Cable shunt admittance was neglected. [8].
- Carson's equations are valid for cable and overhead line impedances.
- End effects were neglected in calculating cable impedances for LV cables [9].
- Aerial Bundle Conductor (70mm2)

  DC resistance (50 °C) - 0.0004973 Ohms/m, Inductive Reactance (50Hz) - 0.000089 Ohms/m
- Aluminium Bare Conductors (60mm^2)

  DC resistance (50 °C) - 0.000505 Ohms/m, Inductive Reactance (50 Hz) - 0.000293 Ohms/m.
- The fault level at the HT side of the transformer was assumed to be 10 kA.
- Spacing between conductors and their erection heights were taken from the CEB Construction Standards.

TABLE III. COMPARISON BETWEEN VOLTAGE VALUES OF THE CASE STUDY AND SIMULATION MODEL

Distance (m)	Results in OpenDSS model			Real Measurements			Error 1	Error 2	Error 3
	Ph A	Ph-B	Ph-C	Ph-A	Ph-B	Ph-C	Ph-A	Ph-B	Ph-C
126	420	418	419	418	421	420	0.48%	-0.71%	-0.24%
150	420	418	420	419	420	420	0.24%	-0.48%	0.00%
176	420	418	420	417	420	421	0.72%	-0.48%	-0.24%
200	421	419	420	419	420	420	0.48%	-0.24%	0.00%
248	421	419	420	419	417	420	0.48%	0.48%	0.00%

B. *Model Validation*

Model validation was done using the measurements taken in the case study given in Section IV-B. A comparison between the voltage values taken from the case study and the simulation model is given in Table III. Errors between voltage values taken from the case study and the simulation model are less than 1 %. Therefore, it was considered that conductor models developed in OpenDSS were accurate enough for further studies.

VI. ANALYSIS OF SIMPLIFIED RADIAL LV NETWORK USING MONTE CARLO SIMULATION TECHNIQUE

A. *Developing Simplified LV Network Model*

From case studies, it was identified that the PV penetration limit must be determined solely by their impact on feeder voltage rise, not by their effects on harmonic levels. Therefore, models were developed only for 50Hz, power frequency.

In this analysis, first, simplified radial LV network models were developed to represent urban, semi-urban, and rural areas in CEB. Network parameters that were validated in the model validation stage were directly applied for these models. Then, Solar PV hosting capacity limits were found by implementing the Monte Carlo simulation technique for them. The following are the additional assumptions made to develop simplified radial LV Network Models.

- Service poles were considered as circuit nodes where all service wires and spur lines are connected.
- PV inverters were modeled as simple constant power generators.
- PV inverters were set to operate at rated power. (snapshot modeling for the worst-case scenario)
- Pole span was assumed to be 30 m.
- Having more than one three-phase roof-top Solar PV to a particular node is highly unlikely.
- In Urban areas, Feeder lengths were assumed to be either 300 m & 510 m.
- In semi-urban areas, the feeder-length was assumed to be 810 m.
- In Rural areas, the feeder-length was assumed to be 1020 m & 1500 m.
- Feeder loading was uniformly distributed along the feeder.
- For low loading cases, feeder loading was assumed to be 16 % of the Power Carrying Capacity of the feeder.
- For medium loading cases, feeder loading was assumed to be 26 % of the Power Carrying Capacity of the feeder.
- For high loading cases, feeder loading was assumed to be 46 % of the Power Carrying Capacity of the feeder.

B. *Assignment of PV Systems to Simplified Radial LV Network Model*

In the Monte Carlo simulation technique, PV systems were assigned to circuit nodes according to a probabilistic model developed based on the latest PV inverter population statistics at the time of research. The number of units by PV inverter capacity for a random sample of size 337 of PV inverters installed islandwide are shown in Fig. 9. To assign single & three-phase inverters for a circuit node, probabilistic models shown in Table IV were developed based on the statistics of the sample.

In Fig. 10, it is shown how PV systems were assigned to each node of the radial LV network model. Monte Carlo Simulation technique was implemented for all OpenDSS LV network models using python scripts. The main objective of using the Monte Carlo technique in this exercise is to find a relationship between the maximum feeder voltage & PV penetration. The algorithm used for the Monte Carlo technique is shown in Fig. 11.

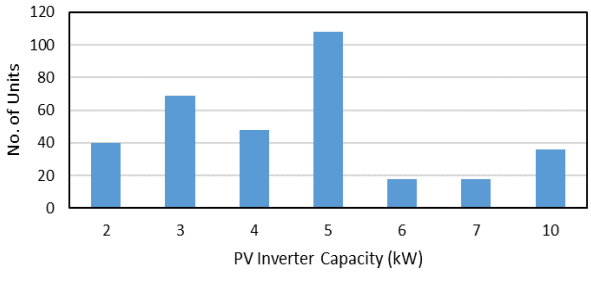

Fig. 9. The number of units vs PV inverter capacity.

TABLE IV. PROBABILISTIC MODELS FOR ASSIGNING SINGLE & THREE-PHASE INVERTERS FOR A CIRCUIT NODE

PV Inverter Rated Capacity(kW)	Probability of Occurrence (p) (Urban, Low tap)	Probability of Occurrence (p) (Rural, High tap)
0.0 (No Solar PV)	$0< p \leq 0.8$	$0< p \leq 0.95$
2.0	$0.8 < p \leq 0.827$	$0.95 < p \leq 0.9566$
3.0	$0.827<p \leq 0.872$	$0.9566<p \leq 0.968$
4.0	$0.827<p \leq 0.944$	$0.968<p \leq 0.986$
5.0	$0.944<p \leq 0.976$	$0.986<p \leq 0.994$
6.0	$0.976<p \leq 0.988$	$0.994<p \leq 0.997$
7.0	$0.988<p \leq 1$	$0.988<p \leq 1$
10.0 (3 phase)	p> =0.9786	p>=0.994

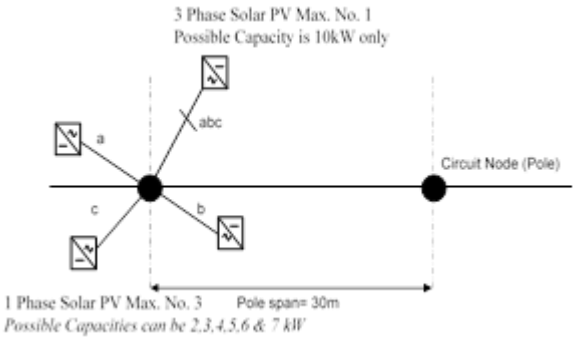

Fig. 10. Assignment of PV systems to each node of the radial LV network model.

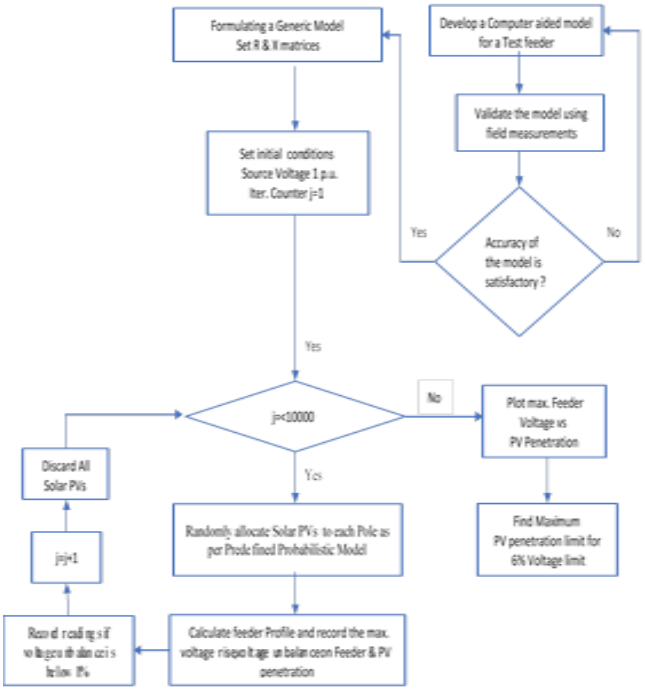

Fig. 11. A flow chart that illustrates the Monte Carlo technique.

C. *Determining the Safest PV Hosting Capacity Limits for Simplified Radial LV Networks*

Safest PV hosting capacity limits for different feeder lengths and loading conditions were found from the maximum phase voltage (p.u.) versus PV penetration (kWp) graphs drawn for each case. One example of such a graph and how the Safest PV hosting capacity limit was derived from that is illustrated in Fig. 12.

In Fig. 12, the worst-case scenario phase voltage level for a specific solar PV penetration level was represented by a blue color point. It is evident from this graph that, as solar PV penetration goes beyond 25 kW, the possibility of rising phase voltage above +6 % of the nominal goes higher whereas if the solar PV penetration level is less than 25 kWp, getting a voltage violation event at any time is highly unlikely. It is also clear that if the solar PV penetration level of the feeder is higher than 50 kWp, an overvoltage event can happen for any solar PV connection arrangement.

Therefore, from this graph, it was observed that for a 500-m length simplified radial network with ABC cables under low loading cases (16 %), the safest solar PV hosting capacity will be 25 kWp whereas the maximum hosting capacity of the feeder will be 50 kWp. Similarly, the safest solar PV hosting capacity for all different feeder lengths and loading conditions can be found from their maximum phase voltage (p.u.) versus PV penetration (kWp) graphs as the above. All the results (safest solar PV hosting capacities) of this Monte Carlo analysis for different feeder configurations and loading conditions are summarised in Table V.

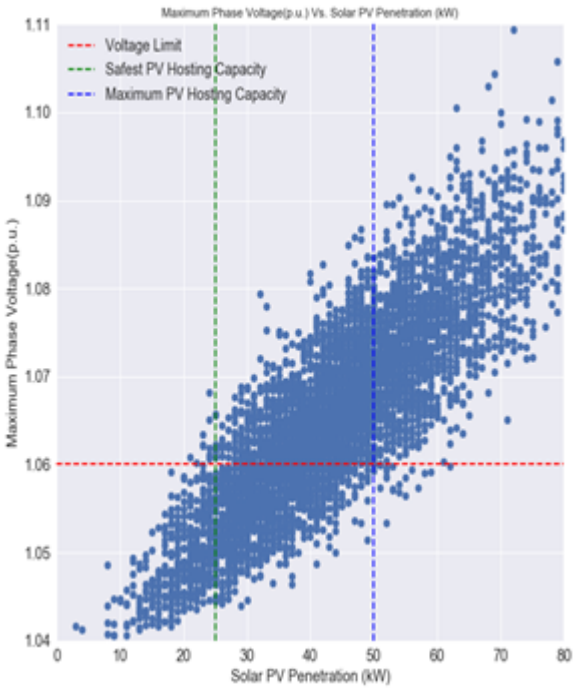

Fig. 12. The safest PV hosting capacity limit for a 500-m long simplified radial LV network with 70-mm^2 ABC cables under low loading case (16 %).

TABLE V. SUMMARY OF RESULTS OF MONTE CARLO ANALYSIS FOR DIFFERENT TYPES OF SIMPLIFIED RADIAL LV NETWORK MODELS

Feeder Length (m)	Present Feeder Loading (%)		
	Low load case 16 (%)	Medium load case 26 (%)	High load Case 46 (%)
ABC cable – Safest solar PV Hosting Capacity in kWp			
Urban areas 300	38	50	70
Urban areas 500	25	30	50
Semi- Urban areas 810	18	24	40
Rural areas 1000	16	22	30
Rural areas 1500	15	17	25
AAC Fly - Solar PV Hosting Capacity in kWp			
Urban areas 300	42	60	90
Urban areas 500	30	40	70
Semi- Urban areas 810	20	27	40
Rural areas 1000	18	24	32
Rural areas 1500	16	18	26

D. Limitations of the Monte Carlo Analysis

Since all the modeling was done for simplified radial LV networks with some general assumptions, the results of this Monte Carlo analysis (Hosting Capacities found) cannot be directly applied for any actual feeder in the CEB network. Even if this technique is used for an actual feeder arrangement with actual load conditions, derived hosting capacity will apply only for that particular feeder, not to any other. Further, this technique cannot be used to conclusively rule out a new roof-top solar PV introduced after its hosting capacity is reached. This is because, as per Fig. 12, even after the hosting capacity is exceeded, it is still possible to have no overvoltage events with some solar PV connection arrangements.

E. Observations of the Monte Carlo Analysis

Even though there are limitations to the Monte Carlo Analysis, the results of this analysis give specific insights on how solar PV generation will impact on the feeder voltage under different load conditions and feeder lengths. For example, from Table V above, it is evident that for any feeder length, the safest solar PV hosting capacity goes up as feeder loading level goes up from 16 % to 46 %.

Therefore, it is evident that the voltage impact of LV connected solar PV goes down as the feeder loading increases. The main reason for this is high feeder loading reduces the reverse power flow, which ultimately can cause voltage rise phenomena at feeder ends. It was also found that conductor type (being Bundle or fly) has a considerable impact on the solar PV hosting capacity. From Table V, it was observed that solar PV hosting capacities are always higher for AAC fly cable than ABC bundle cable in all cases. From Table V, it is also evident that as total feeder length increases, the safest hosting capacity limit of the feeder comes down under any case.

VII. CONCLUSION AND RECOMMENDATIONS

From the Monte Carlo analysis, it can be clearly shown that the presence of solar PV systems in LV feeders will increase the probability of voltage rise above 6 % of nominal voltage (230 V). However, the Monte Carlo analysis cannot be used to determine hosting capacities for actual feeders in CEB's LV network. From the observations, it can be concluded that the relative voltage rise from the nominal voltage at any point is always proportional to P*R where R is the equivalent source resistance between the substation and solar PV system. P is the injected active power of the solar PV system.

From case studies, it was identified that the setting of the over-voltage protection, as a part of the inverter protection settings, is playing a vital role in preventing sustained over-voltages. In Sri Lanka, it is required that PV inverters trip once the regulatory overvoltage limit is exceeded (6 % of nominal voltage (230 V)). However, from the observations, it can be concluded that the use of overvoltage protection for voltage control always leads to nuisance tripping of PV inverters.

Both from case studies and simulation modeling, it can be shown that the uneven power injection of single-phase solar PV systems can cause the voltage to unbalance in the feeder. However, this issue can be further aggravated by already existing voltage unbalance issues of CEB supply. For three-phase solar PV systems, voltage unbalance was not found to be an issue.

By considering the results of case studies and simulation modeling, the following measures are recommended to mitigate voltage issues and to improve PV hosting capacity in CEB LV networks.

- Introduce Battery Storage System (BSS) for roof-top solar PV systems. (reduces reverse power flow)
- Introduce PV hosting capacity limits in LV networks.
- Limit single-phase PV inverter capacity. Size above the limit shall have the 3-phase configuration. (reduces uneven power flow)
- Permit only grid-tie inverters having active & reactive power controlling algorithms.

REFERENCES

[1] A. E. Mohamed and Z. Zhao, ''Grid-connected photovoltaic power systems: Technical and potential problems—A review," *Renewable and Sustainable Energy Reviews*, vol. 14, no. 1, pp. 112 – 129, 2010.

[2] S. Cobben, B. Gaiddon, H. Laukamp, ''Impact of Photovoltaic Generation on Power Quality in Urban Areas with High PV Population (Results from Monitoring Campaigns)" Availble [online] https://www.academia.edu, accessed June 2018.

[3] T, Aziz and N. Ketjoy, "PV Penetration Limits in Low Voltage Networks and Voltage Variations," *School of Renewable Energy Technology, Naresuan University,* Vol. 5, pp. 16788 - 16789. August 2017

[4] S. Pukhrem, M. Basu, M. F. Conlon, and K. Sunderland, ''Enhanced network voltage management techniques under the proliferation of roof-top solar PV installation in low-voltage distribution network.," *IEEE Journal of Emerging and Selected Topics in Power Electronics*, vol. 5, no. 2, pp. 681 – 694, June 2017.

[5] A. F. Povlsen, ‘‘Impacts of power penetration from photovoltaic power systems in distribution networks,” Task V, Report IEA-PVPS T5-10: 2002, February 2002.

[6] C. Po-Chen, ‘‘Analysis of voltage profile problems due to the penetration of distributed generation in low-voltage secondary distribution networks*,” IEEE Transactions on Power Delivery*, vol. 27, no. 4, pp. 2020 - 2028, September 2012.

[7] M. Zeraati, M. E. Hamedani Golshan, and J. Guerrero, ‘‘Distributed control of battery energy storage systems for voltage regulation in distribution networks with high PV penetration,” *IEEE Transactions on Smart Grid*, vol. 9, no. 4, pp. 3582 – 3593, December 2016.

[8] W. H. Kersting, Distribution System Modeling and Analysis, Boca Raton: CRC Press, 2012, p. 439.

[9] J. R. Carson, “Wave propagation in overhead wires with ground return”, *Bell System Technical Journal*, no. 5, pp. 539–554, 1926.

Energy Consumption Comparison of Inverter and Non-Inverter Refrigerators

K. G. R. F. Comester
Research and Development Branch
Ceylon Electricity Board
Colombo, Sri Lanka
dgmrd@ceb.lk

A. D. J. Rupasinghe
Research and Development Branch
Ceylon Electricity Board
Colombo, Sri Lanka
cedsm@ceb.lk

A. L. Deshapriya
Research and Development Branch
Ceylon Electricity Board
Colombo, Sri Lanka
ee2dsm.cs@ceb.lk

***Abstract*— This study focuses on the comparison of energy consumption of inverter and non-inverter refrigerators. Modern refrigerators consist of digital inverter compressors. They are said to ensure high efficiency and consistent temperature inside the refrigerator. Even though these refrigerators known to provide significant cost savings due to less energy consumed compared to non-inverter refrigerators, studies in energy consumption difference between two types of refrigerators are limited. The study revealed that the average energy consumption of inverter refrigerators is 27.76 % less than that of non-inverter refrigerators; and the value is highly dependent upon the manufacturing quality of the refrigerator.**

Keywords— cost, energy, inverter, non-inverter, refrigerators

I. INTRODUCTION

Refrigerators are used to store food at a temperature of about 3 to 5 °C (37 to 41 °F) to prevent it from spoiling. Frequently, a refrigerator is combined with a small freezer, where food is kept frozen at below 0°C. Refrigerators are also used in food processing and retailing and other applications e.g. for storing vaccines and medical products.

Technically, the two main types of refrigerators are compression and absorption refrigerators. Most refrigerators today use an electric compressor running on electricity obtained from the grid, and a closed vapor compression cycle with a refrigerant (formerly ammonia or chlorofluorocarbons). The temperature inside the refrigerator is cooled as the refrigeration agent, which is in a high pressure, liquid state vaporizes and absorbs heat from its environment.

There are two types of compression refrigerators. They are inverter and non-inverter refrigerators. Unlike the standard single-speed compressor (Non-Inverter refrigerator), which is either off or operating at full speed, the digital inverter compressor is almost always on but can operate at different speeds. This ensures high efficiency and consistent temperature inside the refrigerator.

As explained above, inverter refrigerators consume less energy compared to non-inverter refrigerators due to the ability to operate at different speeds. Everyone agreed with the concept of low energy consumption of inverter refrigerators. But there was not a comparison of the energy consumption difference between two types of refrigerators in numbers. This study focuses on the comparison of energy consumption of inverter and non-inverter refrigerators.

II. LITERATURE SURVEY

A. Usage of Refrigerator

Refrigeration has grown to become the most essential food storage technique in developed countries. As key features of any kitchen, refrigerators, and freezers form an integral part of the home appliances market. Makers of some of the most popular refrigerator brands—like Whirlpool, Samsung, LG, Panasonic, Hitachi, Sharp, and Haeir are among the leading household appliance companies worldwide.

Refrigerators and freezers may either be free-standing or built into a kitchen. Refrigerators may also be combined with freezers, stacked with either the refrigerator or freezer above, below or side by side. Other types include the French door style and the less expensive compact refrigerator, built to save space but with less storage space inside. As an example, Around 10 million units of refrigerators are sold each year in the United States, and shipment of freezers within the U.S. amount to more than two million units every year and around 8 million units of refrigerators are made in each year in India.

B. Cooling Load

The cooling load on the refrigeration system determines the size of the refrigeration plant and therefore its power consumption. The smaller the load, the lower the power consumption. The load is usually made up of several different components. You may be able to reduce or eliminate one or more of these.

C. Energy Consumption

Several studies and institutions have already examined how consumer handling of refrigerators influences their energy consumption and how this energy consumption can be reduced. The following factors which allegedly may have an impact on energy consumption were mainly investigated in previous studies:

- Room/ambient temperature
- Compartment temperature of the refrigerator
- Door openings
- Additional heat load by warm food placed in the refrigerator
- Filling level

III. Inverter refrigerators Vs non-Inverter refrigerators

For decades, refrigerators had single-speed compressors that were always either off or on. A compressor is the engine that powers the refrigeration cycle, moving refrigerant through the inner and outer heat exchange pipes. With a single-speed compressor, when the temperature inside the refrigerator reaches above a certain temperature, the compressor suddenly switches on – a noise almost everyone is familiar with. The single-speed compressor operates at full power, producing enough cool air until the temperature has sufficiently decreased before abruptly shutting off.

Nowadays refrigerators have digital inverter compressors instead of conventional refrigerators. (a compressor that can operate at variable speeds because it is operated with a digital inverter). Unlike the standard single-speed compressor, which is either off or operating at full speed, the digital inverter compressor is almost always on but can operate at different speeds. This ensures high efficiency and consistent temperature inside the refrigerator. It also results in significant cost savings, a reduced carbon footprint, less noise, and a longer lifespan for the compressor. The digital inverter compressor is one of the most important innovations in the history of refrigerators and food preservation.

An inverter refrigerator unit has a variable speed compressor motor that adjusts the refrigerant flow inside the unit to control the cooling and heating capacity as required. The speed of the compressor motor in an inverter unit is directly proportional to the frequency of the power supply. It uses a variable-frequency sensor to control the speed of the motor which regulates the refrigerant flow inside the unit to provide just the right amount of cooling or heating as needed. This eliminates the frequent start-stop cycles thereby increasing the energy efficiency of the unit in the long run.

A non-inverter refrigerator unit has a fixed speed compressor motor. Unlike inverter units, they work on an "all or none" principle meaning the compressor automatically goes on and off rather than running at a full speed all the time. The compressor automatically switches off when the desired temperature is reached and starts again when the temperature increases. Because of the frequent on-off cycles, the compressor always works at high power which creates a whole lot of noise while running thereby consuming more electricity at times making them less energy efficient than their inverter counterparts. An inverter, in general, is a device to change the type of current from AC to DC or vice-versa. In terms of refrigerator units, an inverter is used to control the power supply frequency of the compressor motor to adjust the cooling/heating capacity of the unit. An inverter refrigerator contains a variable speed compressor that regulates the temperature to provide just the right amount of cooling and heating as needed. A non-inverter refrigerator, on the contrary, has a fixed speed compressor that works on an "all or none" principle meaning it switches on and off when required.

IV. Methodology

Since the established testing procedures were limited, a new testing procedure to compare these refrigerators in relation to energy consumption has to be established concerning available SLS standard 1230:2003 for refrigerators, as follows,

Standard MADI test pieces with dimensions and weight $200 \times 100 \times 50$ mm^3 and 1 kg, respectively, have been used to load refrigerators (c.f., Fig. 1). A plastic bush is already inserted in the middle of the test packages. In this way, we can preserve the thermocouples wires to measure the temperature inside the test piece.

- Refrigerators were loaded up to 12 kg and 9 kg of test pieces according to the volume of refrigerators. Approximately 50% of the freezer volume was filled using test pieces.
- The test was conducted under controlled ambient conditions of 28 ^{o}C and 60 – 70 % relative humidity inside the test chamber.
- Then the electricity supply was given to refrigerators.
- Temperature Readings were taken at different regulator positions and adjusted the regulator position where the average temperature of the freezer is -15 ^{0}C and temperature of fresh food compartment is 5 ^{0}C or the nearest below temperature reading which can be achieved by adjusting regulator settings.
- When the temperature inside the freezer was -15 ^{0}C and temperature inside the fresh food compartment is 5 ^{0}C, thermocouples were inserted to test pieces.
- Then some time was given to stabilize the temperature of test pieces to -15 ^{0}C.
- Test pieces of 3 kg were added to the freezer after stabilizing the temperature of test pieces to -15 ^{0}C with 40 seconds of a door opening.
- The energy required by the refrigerator to cool the newly added test pieces from room temperature to -15 ^{0}C was measured.

Six number of refrigerators from three different manufacturers were tested in Refrigerator Testing Laboratory of National Engineering Research & Development (NERD) Centre, Sri Lanka. Summary of refrigerator classification as per SLS 1230:2003 is given in Table I. Models represented by 2, 3, and 5 were inverter refrigerators while others were non-inverter refrigerators.

Fig. 1. MADI test piece

TABLE I. REFRIGERATOR CLASSIFICATION

Model	Refrigerator Class
1	4
2	4
3	4
4	5
5	5
6	4

3. The energy consumption of refrigerators highly depends on the Regulator position of the refrigerator. Therefore, it is required to set the regulator position correctly to compare the energy consumption of refrigerators.
4. The percentage energy consumption difference of averaged energy consumption of inverter and non-inverter refrigerators is 27.76%.
5. Percentage energy consumption difference of best energy consumption inverter refrigerator and worst energy consumption non-inverter refrigerator is 47.77%.

TABLE II. NAME PLATE INFORMATION

Manufacturer	**A**	**A**	**B**	**C**	**C**	**C**
Model	1	2	3	4	5	6
Colour	Silver Strips	Grey Strips	Silver grey	SS color	silver grey	silver grey
Product dimensions (mm)	540x712x1480	540x712x1480	not mention	not mention	not mention	not mention
Net weight(kg)	51.5	51.5	52	39.5	46	46
Capacity (l)	250	250	251	176	220	220
Refrigerant	R600a (55g)	R600a (55g)	R600a (46g)	R600a (40g)	R600a (54g)	R600a (54g)
No of Doors	2	2	2	2	2	2
Automatic(A)/Manual (M) Defrost	A	A	A	M	A	A
Voltage/Frequency	220/240/50Hz	220/240/50Hz	220V/50Hz	230/240/50Hz	230/240/50Hz	230V/50Hz
Current (A)	0.5	0.5	1.0	0.32	0.32	5.0
Motor Input (W)	80	80	100	72	81	81

V. RESULTS

Normally the information given in the nameplate is approximate values as shown in Table II, and their calculation methods are different from manufacturer to manufacturer. Therefore, those parameters were measured and calculated as given in Table III. Further, measured energy consumption values and calculated energy consumption per unit volume per ^{0}C values are given in Table IV

A summary of the test is included in Table IV. Calculated energy consumption per unit volume per ^{0}C values of each refrigerator was taken to compare the energy-related performance of refrigerators.

VI. CONCLUSION

1. It can be concluded that inverter refrigerators consume less energy than non-inverter refrigerators.
2. Even though inverter refrigerators consume less energy, the percentage difference in energy consumption is heavily dependent on the quality of the refrigerator.
6. Percentage energy consumption difference of best energy consumption inverter refrigerator and best energy consumption non-inverter refrigerator is 12.24%.
7. The percentage energy consumption difference between the worst inverter and worst non-inverter refrigerator is 40.48%.
8. It is noted that the energy consumption of some inverter refrigerators is not at a satisfactory level and also the energy performances of some non-inverter refrigerators are up to the level of inverter type refrigerator.

TABLE III. MEASURED AND CALCULATED PARAMETERS

Refrigerator Model (Brand)	**1 (A)**	**2 (A)**	**3 (B)**	**4 (C)**	**5 (C)**	**6 (C)**
Type	Non Inverter	Inverter	Inverter	Non Inverter	Inverter	Non Inverter
Regulator Position; Freezer	4	5	Optimal	5	8 dots from coldest	8 dots from coldest
Regulator Position: Fresh Food Compartment	4	3	3	NA	11 dots from coldest	11 dots from coldest
Test Chamber Set temperature (^{0}C)	28	28	28	28	28	28
Loading Detail	12kg	12kg	12kg	9kg	12kg	12kg
Time Duration (h:s) to reach required temperature	13.25	17.88	12.78	21.26	18.75	18.83
Energy Consumption, Ec (Wh)	953.5	967.82	981.78	879.14	848.44	1443.18
Average Freezer Temperature (^{0}C)	-16.08	-15.65	-17.10	-10.50	-14.70	-17.70
Average Fresh Food Comp.Temperature (^{0}C)	6.08	0.36	3.58	-0.18	4.62	5.08
Measured Volume - Freezer Vf (l)	56.00	56.00	59.00	33.21	55.13	55.13
Measured Volume Fresh Food Compressor Vc (l)	183.00	183.00	189.00	132.57	145.39	145.39
Measured Total Volume (l)	**239.00**	**239.00**	**248.00**	**165.79**	**200.51**	**200.51**
V1=Vf x Kf + Vc x Kc*	6479.56	7502.52	7276.28	5014.70	5753.04	5851.54
Energy consumption per unit volume per 1^{0}C, (Ec/V1)	**0.147**	**0.129**	**0.135**	**0.175**	**0.147**	**0.247**
Combine Uncertainty	0.005	0.005	0.005	0.005	0.005	0.005

* K_f is taken as (28 - $T_{f)}$ and Kc as (28 – T_c)

TABLE IV. SUMMARY OF THE TEST

Model (Manufacturer)	**1 (A)**	**2 (A)**	**3 (B)**	**4 (C)**	**5 (C)**	**6 (C)**
Type	Non Inverter	Inverter	Inverter	Non Inverter	Inverter	Non Inverter
Total Volume (liters)	239	239	248	166	201	201
Average Freezer Temperature (^{0}C)	-16.08	-15.65	-17.1	-10.5	-14.7	-17.7
Average Fresh Food Comp. Temperature (^{0}C)	6.08	0.36	3.58	-0.18	4.62	5.08
Energy consumption per unit volume per 1^{0}C, (Ec/V1)	**0.147**	**0.129**	**0.135**	**0.175**	**0.147**	**0.247**

Average energy consumption per unit volume per 1^{0}C, (Ec/V1) for inverter refrigerators	0.137
Average energy consumption per unit volume per 1^{0}C, (Ec/V1) for non-inverter refrigerators	0.190
Percentage difference of averaged energy consumption of inverter and non-inverter refrigerators	27.76%
Percentage difference of best energy consumption of inverter refrigerator and worst energy consumption of a non-inverter refrigerator	47.77%
Percentage difference of best energy consumption of inverter refrigerator and best energy consumption of a non-inverter refrigerator	12.24%
The percentage energy difference between worst inverter and worst non-inverter refrigerator considering the energy consumption	40.48%

ACKNOWLEDGMENT

The authors are thankful for the NERD Centre and its staff for the provision of testing facilities and expert support throughout this study.

Impact of Three-Hour Power Discontinuation of Refrigerators on Microbiological Stability of Food

K. G. R. F. Comester
Research and Development
Ceylon Electricity Board
Colombo, Sri Lanka.
dgmrd@ceb.lk

A. D. J. Rupasinghe
Research and Development
Ceylon Electricity Board
Colombo, Sri Lanka.
cedsm@ceb.lk

A. L. Deshapriya
Research and Development
Ceylon Electricity Board
Colombo, SriLanka.
ee2dsm.cs@ceb.lk

Ilmi Hewajulige
Food Technology Section
Industrial Technology Institute
Colombo, Sri Lanka.

Wasundara Divisekera
Food Technology Section
Industrial Technology Institute
Colombo, Sri Lanka.

Samantha Madage
Food Technology Section
Industrial Technology Institute
Colombo, SriLanka.

Sudeepama Walliwala
Food Technology Section
Industrial Technology Institute
Colombo, Sri Lanka.

Udayani Binduhewa
Food Technology Section
Industrial Technology Institute
Colombo, Sri Lanka.

***Abstract*— This paper provides an investigation into refrigerated food quality in power discontinuation scenarios. Standardized methods were followed in food preparation, testing, and measurement. Generalized refrigerator usage was simulated emulated with the introduction of a three-hour-discontinuation of power. Temperature measurements inside the compartments have shown drastic variations within power discontinuation while consuming elongated periods to normalize after power restoration. Furthermore, the investigation with Aerobic Plate Count and, Yeast and Mold Count has shown the increased growth of microorganisms (bacteria and mold) upon food during the period of temperature normalization of the refrigerator which could lead to serious risk of food safety.**

Keywords— food safety, microorganisms, power discontinuation, refrigerators, temperature

I. INTRODUCTION

Refrigerators are designed to provide suitable temperatures for maintaining chemical and microbiological stability of food thus improving the shelf life and establishing food safety. Refrigerated storage is essential for food items prepared at home which are intended for short term storage and opened commercial food packages, especially belonging to the low acid food category. Hence, this is an essential food storage system used in almost every household now.

As the refrigerator maintains a temperature below the ambient room temperature, it lowers the rate of bacterial multiplication and metabolism thus reducing the food spoilage and intoxication. Using refrigerators prevents the food from getting entered into the danger zone as described by USDA Food Safety and Inspection Service. In the "Danger Zone" (4 °C - 60 °C), bacteria grow more rapidly, doubling in number and releasing their metabolic products to the food resulting in food poisoning and food intoxication respectively. Therefore, maintaining the proper temperature range inside the refrigerator is required and it can be fulfilled only by a continuous supply of electricity.

Due to the high cost of electricity, currently, most of the refrigerator users discontinue the electricity supply for a few hours (2-3 hours) during peak electricity consumption hours to reduce the consumption of electricity. The objective of this study is to investigate the effect of three-hour-power discontinuation of refrigerators on food safety in terms of microbiological stability under laboratory conditions.

II. METHODOLOGY

The laboratory experiments were conducted using two refrigerators provided by the Ceylon Electricity. One refrigerator was used as the control (without power discontinuation), and the other was the test refrigerator (with power discontinuation). All the sample preparations were carried out using fresh commodities purchased from the local market and potable water under hygienic conditions at the Fruits and Vegetables processing laboratory of the Food Technology Section.

All the microbiological analyses were conducted in a strict aseptic environment using the Class II Biological safety cabinet at the Microbiology Laboratory of Food Technology Section. For the microbiological analysis, Himedia (India) microbiological media and all sterilized glassware were used.

Food commodities were selected based on their consumption stage.

- Cooked refrigerated food: Cooked rice, Cooked dhal curry
- Raw frozen food: Fish
- Raw refrigerated food: Grated coconut
- Ready to Serve frozen food: Ice cream
- Ready to serve refrigerated food: Sterilized milk
- Pre-cooked frozen food: Sausages

Standardized procedures were followed to prepare food used for each experiment (ingredient quantities and cooking conditions). Both refrigerators were given similar conditions including identical samples of prepared food and the only variation is the power discontinuation in the test refrigerator. All the experiments were repeated thrice to confirm the reproducibility of data.

Fig. 1. Thermocouple arrangement of empty refrigerator.

To measure the temperature distribution of various compartments of the empty refrigerator, a calibrated thermocouple was used. The test compartments included proximal and, distal ends from the freezer, the door of the freezer, fresh basket, egg rack, and bottle rack, etc. The refrigerators were given continuous electricity supply and temperatures were recorded every five minutes for five consecutive hours, using an analog data recorder as shown in Fig. 1. The temperature measurements were recorded, where the electricity supply was disconnected in the test refrigerator for three hours.

The test food commodities were stored in both test and control refrigerators as shown in Fig. 2. The experiment was conducted for 72 consecutive hours. Electricity supply was disconnected in the test refrigerator for three hours in each 24-hour cycle during the study. The doors of the refrigerators (both test and control) were kept open for 30 seconds every 30 minutes during the three-hour-period of power disconnection. A door opening was conducted to facilitate the usual household condition in vitro.

Fig. 2. Thermocouple arrangement of refrigerator loaded with food.

The temperature measurements were recorded according to the conditions specified in aforesaid standards in Section II, Microbiological status of the commodities stored in both test (with electricity disconnection) and control (with continuous electricity) refrigerators were determined. The samples were drawn aseptically into pre-sterilized bags and proceed to the microbiological analysis. Microbiological analysis was conducted according to the following specifications,

- SLS 516 part I: 1991 General Guidance for Enumeration of Micro-organisms Colony Count Technique at 30 °C (1st Revision).
- SLS 516 Part II: 1991 Enumeration of Yeasts and Moulds (1st Revision).

For the enumeration of Aerobic Plate Count SLS 516 part I, and for the enumeration of Yeasts and Moulds, SLS 516 part II was followed. The initial microbiological count was taken before the storing of food commodities in both test and control refrigerator. After storing the food commodities in the refrigerators, samples were drawn aseptically at 24 hrs and 72 hrs followed by microbiological analysis.

III. Results and Analysis

A. Compartment Temperature Test

Temperature variation in the control and test refrigerators during power interruption is illustrated in Fig. 3. Temperature measurements inside the freezer are represented by T1 – T4, T6, T8, T9, T12 while the temperature measurements of refrigerator door are represented by T5, T7, T10, T13, T14 with T16 denoting the room temperature.

Results revealed that the three-hour power interruption significantly affects the chamber temperature. Drastic temperature fluctuation was observed in doors of compartments, normal refrigerator compartment (from 4 ^{0}C to 24 ^{0}C), and freezer compartment (from -20 ^{0}C to 10 ^{0}C). It was observed that both the refrigerator and freezer compartment took about three hours to reach the set temperature.

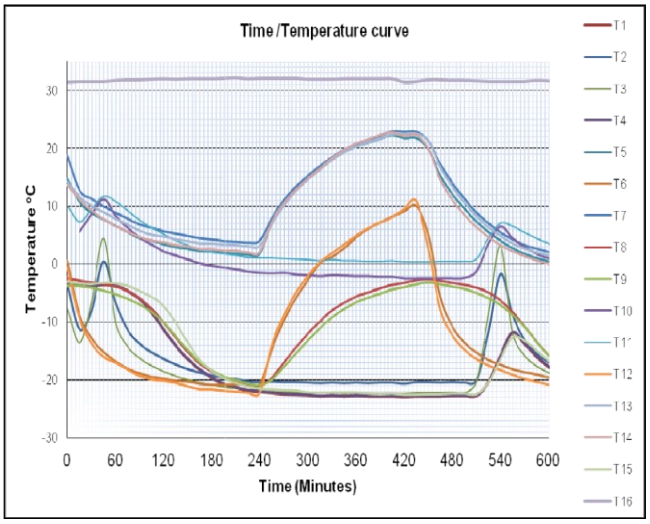

Fig. 3. Chamber temperature variation in the control and test refrigerators during a power interruption.

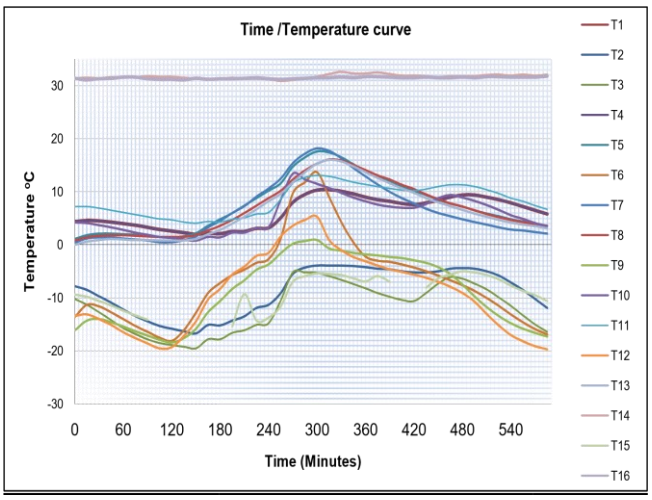

Fig. 4. Effect of power interruption and door openings on inside temperatures (food and compartments).

Temperature variation of food and refrigerator chambers during the power interruption and subsequent door openings are illustrated in Fig. 4. Temperature value representation is given by freezer food (T1-T3, T9, T15), refrigerator food (T4, T5, T10, T11, T13), freezer chamber (T6, T12), refrigerator chamber (T5) and room temperature (T14, T16).

TABLE V. MICROBIOLOGICAL ANALYSIS- AEROBIC PLATE COUNT OF STORED TEST FOOD ITEMS

Sample	Time duration	Test refrigerator cfu/g or cfu/ml	Control refrigerator cfu/g or cfu/ml
Cooked Rice	Initial	$32x10^3$	$32x10^3$
	After 24 hrs	$120x10^4$	$60x10^3$
	After 72 hrs	$160x10^5$	$145x10^4$
Cooked Dhal	Initial	$328x10^4$	$328x10^4$
	After 24 hrs	$19.5x10^7$	$12.5x10^5$
	After 72 hrs	$37x10^7$	$33.5x10^5$
Coconut	Initial	$3x10^4$	$3x10^4$
	After 24 hrs	$40x10^8$	$18x10^7$
	After 72 hrs	$76x10^8$	$148 x10^7$
Milk	Initial	$56x10^1$	$56x10^1$
	After 24 hrs	$92x10^4$	$23x10^3$
	After 72 hrs	$115x10^5$	$62x10^3$
Ice Cream	Initial	$75x10^2$	$75x10^2$
	After 24 hrs	$110x10^7$	$87x10^3$
	After 72 hrs	$300x10^7$	$200x10^3$
Sausages	Initial	$16x10^3$	$16x10^3$
	After 24 hrs	$4x10^8$	$28x10^3$
	After 72 hrs	$300x10^8$	$39x10^3$
Fish	Initial	$122x10^4$	$122x10^4$
	After 24 hrs	$45x10^7$	$34x10^6$
	After 72 hrs	$60x10^{10}$	$43x10^7$

A similar pattern of temperature variation is followed in the refrigerator tested with the food commodities and door openings. However, it required more than six hours to reach the set temperature after power re-continuation. Furthermore, even after power re-continuation, the core temperatures of the food commodities were observed to be in the danger zone (about 15 ^{0}C) for more than three hours enabling the fast microbial multiplication thus creating a food safety risk.

B. Microbiological Analysis of Food

Results of the Aerobic Plate Count (APC) and, Yeast & Mold Counts (Y&M) observed during the microbiological analysis of the test commodities are given in Tables I and II, respectively.

The results demonstrated that power discontinuation for three hours has a significant negative effect on the total bacterial count of the samples indicating the increase of the count. This may alter the keeping quality (shelf life) and affect food safety by encouraging the growth of pathogenic bacteria in the group of food spoilage and food intoxication.

The increase of total bacterial count will make chemical and rheological changes in the food making the food unpleasant to the consumers by changing its typical flavors, odors, and color pigments. The results of 72 hours study revealed that continuous power disconnection had affected the total microbiological scenario of the food.

TABLE VI. MICROBIOLOGICAL ANALYSIS- YEAST & MOLD COUNT OF STORED FOOD ITEMS

Sample	Time duration	(Y&M) Test	(Y&M) Control
Cooked Rice	Initial	$13x10^3$	$13x10^3$
	After 24 hrs	$33x10^4$	$20x10^4$
	After 72 hrs	$48x10^4$	$23x10^4$
Cooked Dhal	Initial	$3x10^4$	$3x10^4$
	After 24 hrs	$11x10^6$	$34x10^4$
	After 72 hrs	$1x10^7$	$39x10^5$
Coconut	Initial	$3x10^4$	$3x10^4$
	After 24 hrs	$25x10^7$	$12x10^7$
	After 72 hrs	$33x10^7$	$29x10^7$
Milk	Initial	$7x10^1$	$7x10^1$
	After 24 hrs	$26x10^3$	$6x10^3$
	After 72 hrs	$107x10^3$	$48x10^3$
Ice Cream	Initial	$2x10^1$	$2x10^1$
	After 24 hrs	$27x10^8$	$5x10^5$
	After 72 hrs	$46x10^8$	$7x10^7$

The results of Yeast and Mold analysis revealed that the fungal and yeast growth increased with the power discontinuation. Since the molds will not make huge chemical or rheological changes as bacteria, it is difficult to recognize visibly the food being contaminated with mold.

However, mold can produce different types of toxins which may be fatal to humans and animals. Therefore, it is essential to reduce the mold count in food during processing and storage to assure consumer safety. When comparing with the initial counts of both APC and Y&M, the 24-hr and 72-hr refrigerated food samples have shown significantly higher counts indicating the safety threat that could be produced by the power discontinuation.

IV. Conclusion

This study revealed that the power discontinuation in refrigerators increases the growth of microorganisms, both bacteria, and mold who are already present in the food; thus creating a serious food safety risk.

The study was conducted in a hygienic laboratory condition with the use of clean refrigerators, clean food storage containers, and sterilized bags for storing food. However, the real situations in household refrigerators are far more unhygienic than the tested environment which could increase the growth of microorganisms further. If the food contaminated with pathogenic bacteria faces such situations of temperature fluctuation, there will be a greater risk of food poisoning and intoxication. The microbiological scenario is different from the refrigerator to the refrigerator and it is purely based on the following factors.

- Cleanliness of the refrigerator
- Different food commodities stored (fresh leafy food, starchy food, sugary food,
- Meat/fish, eggs with fecal matter, etc)
- Frequency of opening the door/s
- Duration of the food kept outside before refrigeration
- Packing and storing methods used (covered or uncovered)
- The duration of the refrigerator door/s is kept open.

This study provides research evidence that the initial microbial load of any food item could be further increased if there is a temperature fluctuation in refrigeration. Therefore, it is recommended to have a continuous power supply to refrigerators to ensure the stable microbiological and chemical condition of food.

Assessment of Lightning Effects on Distribution Network and Finding Feasible Solutions for High Lightning Prone Areas

Navodana Kankanamge
New Kelani Bridge Project
Ceylon Electricity Board
Colombo, Sri Lanka
navodanak@yahoo.com

Praneeth Jayaweera
New Kelani Bridge Project
Ceylon Electricity Board
Colombo, Sri Lanka
Praneeth.era@gmail.com

***Abstract*— Lightning impulse currents have high magnitudes in the range up to few hundreds of kA. It has been recognized that the main cause for lightning damages on the distribution network of Sri Lanka is, high impulse impedance of the surge arrestor grounding system. The inductance of the metal parts of the earth electrode is usually neglected when considering the earth impedance of power frequency at 50 Hz. However, the inductance becomes an important parameter when the current flow rate is high in the range of kA/µs. The overall effect of the impedance depends on the magnitude of the dominating effect during lightning. The main objective of this project is to reduce impulse impedance of the earthing system by improving the backfill material.**

Keywords— backfill, grounding, parallel rods, surge current, surge protective devices

I. INTRODUCTION

A tropical country like Sri Lanka has often suffered from lightning, especially in high lightning prone areas in hill countryside. Utilities have to spend more on maintenance and replacement work due to lightning damages. Surge arrestors and body earth grounding system performs the most important role of protection of distribution network including transformers, the most expensive element of the distribution system. To facilitate good protection, the quality of the grounding technique is mandatory although it depends on many uncontrollable parameters such as native soil resistivity and compactness.

In Sri Lanka, the Ceylon Electricity Board (CEB) has major permits to generate, transmit, and distribute electrical power utilities throughout the country. The electrical power distribution divisions of CEB consist of 33 kV medium voltage power distribution lines, 400 V low voltage power distribution lines, and the 33 kV to 400 V distribution transformers. Distribution transformers are located everywhere in the countryside since the domestic voltage level shall be maintained up to the accuracy of ± 6 %. The length of the low voltage electricity distribution lines was generally not exceeding 1,800 m from the respective distribution transformer.

In the distribution network, the step-down power transformer is the most expensive element. Transformer protection must pay significant attention to reduce maintenance costs. There are two main schemes for the protection of a distribution transformer. One is Drop-Down-Lift-Over (DDLO) fuses and these fuses protect the transformer by overcurrents. The second one is surge arresters which are used to ground over-voltage transients appear due to external incidents such as lightning and switching impulses. However, the effectiveness of the grounding system is a critical factor for the protection of the transformer. In this research, root causes for lightning damages to distribution network are identified and adequate preventive solutions are proposed.

The potential at a given height with respect to the ground was considered as V=IR+L (dI/dt), Where 'R' is the resistance of the ground conductor, 'L' is the inductance and 'I' is the current due to lightning strike. When calculating voltage drops along the down conductor, it shows high voltage in the range of 10^9 V experience due to the inductance of the down conductor, but the voltage drop due to the resistance shows the range of 10^4 V for the lightning strike of 50 kA/µs.

Grounding techniques have been detailed in the "Guideline for Distribution System Earthing (Part 1 -1998)", in CEB. In that guideline, it was recommended to use a cylindrical concrete block of 0.3 m radius and for the height of the earth rod for the soils having resistivity less than 200 Ωm. Nowadays, the common practice of grounding of a distribution transformer is connecting the disconnector ends of each three surge arrestors desperately to the transformer body by using a shorter and insulated bunch of copper-coated thin steel wires. One end of 50-mm^2 or 70-mm^2 insulated copper earth wire is connected to the transformer body and the other side is connected to the earth electrode. Exothermic welding or mechanical compression bonding is widely used to connect earth wire and earth electrode. Seventeen-mm or 18-mm diameter, 1.2-m length copper-clad steel earth electrode is used with reinforced concrete encased backfilling as grounding terminal but there is no specification mentioned for the composition of concrete. The diameter of the structure is 0.6 m. Usually, a separate earth electrode is connected to the grounding of the neutral point to maintain less than 25-Ω resistance. Surge arrestor grounding terminal is not more than 10-Ω resistance; parallel earth electrodes are used to achieve the requirement.

Normally dc resistance is the only parameter that is usually checked in grounding systems. It is understood that an acceptable range of dc resistance of the grounding system is not adequate and it does not give complete assurance in a high lightning prone area. Since the inductance of the grounding path plays a major role in the damage by lightning impulse, it is recommended to reduce the total inductance of the grounding system including the earth terminal.

The current rating of the existing surge arrestors of the 33-kV distribution network is 10 kA. However, it was found that the maximum protection of the surge arrestors is not given to the network due to poor ground connectivity. Hence the best solution to minimize lightning damages to the distribution network is placing an improved grounding system for surge

arrestors in critical locations. The grounding system shall consist of low resistive and inductive down conductor and effective cylindrical backfill encased earth rod.

While analyzing the recorded past lightning damaged incidents in the field, it is recommended to continue the shortest possible length of 50-mm^2 or grater copper earth cable. However, to reduce the inductive effect, a cable contained hair conductor strands will give better results while maximizing the skin effect. 12-T pressured crimping connectors have been given better results in the filed than other types. Copper clad steel earth electrode of 18-mm diameter and 1.2-m length can be used as the earth terminal.

This research is directed to find cheap and effective backfilling material which will provide a long term low impedance to the lightning discharge. The composition of the backfill mixture is investigated. Meanwhile, the research identified the most effective dimensions for an earth pit and it is validated by considering cost-effectiveness and the quality of the grounding terminal.

The main objective of this research is to enhance the distribution transformer grounding system while replacing the native soil by moisture-rich, low resistive backfill material by utilizing fly ash; the major by-product of Lakvijaya Power Station, Norochchole for productive usage. Hence this research evaluates the usage of hybrid backfill-electrolytic grounding techniques for distribution transformer locations in high lightning probability and having low native soil resistivity.

II. Lightning Damages and Grounding Systems

Grounding is provided to connect some parts of electrical equipment and installations or the neutral point of a power system to the earth. This provides dispersing paths for fault currents and lightning currents to stabilize the potential and to act as a zero potential reference point to ensure the safe operation of the power system and electrical equipment as well as the safety of power system operators and other persons. Grounding is achieved by grounding devices buried in the soil. The resistance of the earth depends on the type and dimensions of the earth electrode, the earth wire, bonding method between the electrode and the wire, soil resistivity, and the bonding agent between the electrode and the soil. The soil resistivity is defined as specific soil resistance. The relationship between soil resistance (R), soil resistivity (ρ), length of the earth rod (l), and the cross-sectional area of the rod (A) is given by (1).

$$R=\rho\, l/A \tag{1}$$

The efficiency of an electrical grounding system is highly dependent on the grounding resistance. The grounding resistance in turn depends on the soil resistivity as well as the shape of the earth electrode. General practices to achieve low grounding resistance include deep driving of electrodes, installation of the concrete-encased ground as well as backfilling with grounding improvement material.

A concrete-encased electrode can achieve good mechanical strength as well as low resistivity. Also, the durability of the grounding device is at a high level when using the concrete-encased electrode. Other positive factors are ease of construction, availability of materials, low labor and material cost, etc. The resistance of the concrete-encased electrode can be determined by (2) [1],

$$R_c = \frac{1}{2\pi L_r}\left\{\rho_s\left[ln\left(\frac{8L_r}{d_c}\right)-1\right]+\rho_c\left[ln\left(\frac{8L_r}{d_r}\right)-1\right] - \rho_c\left[ln\left(\frac{8L_r}{d_c}\right)-1\right]\right\} \tag{2}$$

Where,

R_c is the resistance of the concrete-encased electrode
L_r is the length of the rod in m
d_r is the diameter of the rod in m
d_c is the diameter of the concrete-encased electrode
ρ_c is the resistivity of the concrete-encased electrode
ρ_s is the resistivity of the soil

TABLE I. Backfilling Options

Type	Material	Performance	Cost	Availability	Difficulties for usage
Clay-Based Backfill Materials	Bentonite	Good	Average	Imported, Available	Easy to use
	Marconite	Excellent	Expensive	Rare	Average
	Lime	Fair	Average	Available	Average
Carbon-Based Backfill Materials	Charcoal	Good	Expensive	Available	Difficult to blend
	Fly Ash	Fair	Cheep	Excess	Easy to use

III. Grounding and Backfilling Options

There are four backfill material types that are widely used to enhance the earth-resistivity in the electricity utility sector namely, Conductive Concrete, Clay-Based Backfill Materials, Carbon-Based Backfill Materials, and Blended Clay-Carbon Backfill Materials. Table I describes candidates which fall into the above categories.

By mixing Clay-Based Backfill Materials with Carbon-Based Backfill Materials, Blended Clay-Carbon Backfill Materials are made. Accordingly, to achieve both water retention capability and low resistivity, it is proposed to find a low-cost Blended Clay-Carbon Backfill Material for the grounding system. Considering the performance, cost, availability, and the difficulties for usage, Bentonite, and Fly Ash are selected for the backfilling material. The best proportions to be mixed with concrete are scientifically found. Some important parameters of Bentonite and Fly Ash are given in Table II.

Bentonite is often used to reduce the resistance between the soil and earth electrode by retaining moisture. The naturally occurring Bentonite compound consists mostly of montmorillonite, minerals and the sodium-based clay. Provided with enough amount of water, it swells up to 13 times its dry volume and will adhere to nearly any surface it touches. It has a hygroscopic nature which enables it to act as a drying agent thus drawing any available water from the soil

TABLE II. Parameters of Bentonite and Fly Ash

Backfilling Material	Bentonite	Fly Ash
Physical State	Solid	Solid
Key Components	Montmorillonite	Zinc
	Quartz	Iron
	Mica	Sulfite
	-	Sulfate
pH Value	8.1 to 10.5	10.8
Bulk Density	801 kg/m^3	1041 kg/m^3

and the surrounding environment, ability to absorb rainwater once installed, and helps increase the conductivity. Bentonite is liable to dry out in a dry environment [2].

Fly ash, the most widely used supplementary cementitious material in concrete, is a byproduct of the combustion of pulverized coal in electric power generating plants. Fly ash use in concrete improves the workability of plastic concrete, as well as the strength and durability of hardened concrete. The spherical shaped particles of fly ash act as miniature ball bearings within the concrete mix, thus providing a lubricant effect. Replacing cement with the same amount of fly ash can reduce the heat of hydration of concrete. It produces equivalent strength at an early age (less than 90 days) that will ultimately exceed the strength of straight cement concrete mixes. The decrease in water content combined with the production of additional cementitious compounds reduces the pore interconnectivity of concrete, thus decreasing permeability. The reduced permeability results in improved long-term durability and resistance to various forms of deterioration.

A. Measurements of Electrical Properties

The concrete-encased electrode grounding device is the common and current practice in the distribution substation grounding system in Sri Lanka. It has good resistivity, good moisture absorption, and retention quality, low corrosiveness, high mechanical strength, long time durability, low labor and material cost, and less time requirement to construction. Also considering material availability and simplicity of implementation, this system is easy to introduce all over the country. Hence, concrete; the mixture of Cement, Sand and Metal were used as a primary backfilling material and Bentonite, Fly Ash, and Coir as an admixture for reducing resistivity.

The electrical property of interest in this study is the resistivity of Concrete and mix of Bentonite, Fly Ash, and Coir with Concrete. The following procedures to measure the resistivity of all samples were adopted in experiments. The standard concrete test cubical mold (c.f., Fig. 1a) with the dimensions of 150 mm x 150 mm x 150 mm was used. Two opposite sides of the mold were fixed with an aluminum plate (with the dimension of 170 mm x 160 mm, folded two 10mm strips about 45 degrees of angle towards from 170mm side as shown in Fig. 1b) to provide a conductive surface for measurement purpose. The mold is then filled up completely with the sample and poked 35 times in every 1/3 potion from a 25-mm diameter steel bar. This is to ensure a uniformly flattened and compressed form of the sample inside the mold.

(a) (b)

Fig. 1. Test specimen mold fabrication: (a) mold and (b) measurement terminals.

TABLE III. COMPOSITION OF SAMPLE NO. 01 TO 04

Sample	Grade	Ratio		
		Cement	Sand	Metal
01	15	1	3	6
02	20	1	2	4
03	25	1	2	3
04	30	1	1	2

Then sample mixture filled cubical molds kept one day for settling. After that sample cubes with aluminum plate were removed from the mold. The sample cubes have been kept at 23 ^{0}C-27 ^{0}C-temperature in an air-conditioned room after removing the mold. Then the resistance has been measured by clipping the two probes of an LCR meter or a Multimeter to the two aluminum plates of each sample cube. The LCR meter or Multimeter was first used to measure the resistance of a known resistor to verify its functionality before being used for this experiment. The measured resistance is approximately equal to the resistance of the mixture. The resistance value displayed at the meter is then used to calculate the resistivity of samples by using (1) [3]. Here the parameters were as follows,

R = Measured resistance value
ρ = Resistivity of the sample
l = Length between two Aluminium plates (0.15m)
A = Area of sample pasted with the Aluminium plate

Therefore, $\rho = 0.15 \times R$.

B. Experiment for Selecting Proper Concrete Composition

The first experiment was used to find the best composition of cement, sand, and metal to achieve the lowest resistivity. In this case, we prepared samples by mixing cement, sand, and metal according to the general concrete grading as shown in Table III. These mixtures were put into the standard concrete test cubical mold.

Then samples were removed from the mold after one day and start to measure resistance value for 28 days. The calculated resistivity values from resistance measurements are shown in Fig. 2.

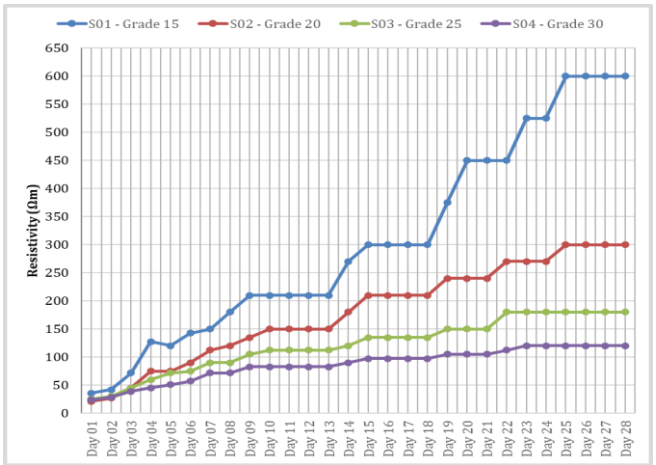

Fig. 2. Resistivity variation of sample No. 01 to 04 with time.

TABLE IV. COMPOSITION OF SAMPLE NO. 05 TO 08

Sample	Ratio					
	Cement	Sand	Metal	Bentonite	Fly Ash	Coir
05	1	*	*	1	-	-
06	1	*	*	0.5	0.5	-
07	1	*	*	-	1	-
08	1	*	*	-	-	0.5

According to Fig. 2, the Grade 30 concrete cube, which contains a high amount of cement has the lowest resistivity readings. In grade 30 concrete the ratio between Cement, Sand, and Metal is 1:1:2. Therefore, this ratio was kept constant and the influence of the Bentonite, Fly Ash, and Coir was found by adding them as shown in Table IV.

Bentonite is a clay-based backfill material and it absorbs water while mixing and increases its volume. It means that the water absorption capacity of Bentonite is very high. First six days it gave better resistivity readings then it became the worst. The sample cubes are placed at 23^0 C - 27^0 C temperature in an air-conditioned room after removing the mold. Moisture content was lower in the environment and Sample No. 06 became dry. The difference between day 01 and day 14 of the Sample No. 06 cube is shown in Fig. 3. It was highly cracked after 14 days. Therefore, the water retention ability of Bentonite is poor when the Bentonite proportion is higher.

Meanwhile, the Fly Ash mixed sample has good mechanical strength but the resistivity level is slightly higher than the Bentonite and Fly Ash mixed sample. Therefore, it was decided to further investigate the promotion between them. Accordingly, Sample 09, 10, and 11 were prepared as per the composition given in Table V.

TABLE V. COMPOSITION OF SAMPLE NO. 09 TO 11

Sample	Ratio				
	Cement	Sand	Metal	Bentonite	Fly Ash
07	1	1	2	0.000	1.000
09	1	1	2	0.125	0.875
10	1	1	2	0.250	0.750
11	1	1	2	0.375	0.625
06	1	1	2	0.500	0.500

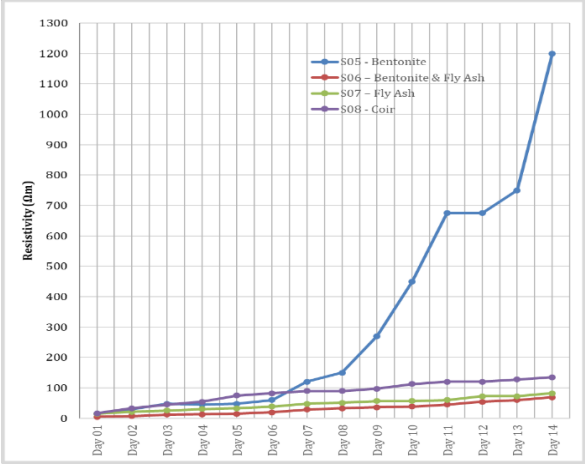

Fig. 3. Resistivity variation of sample No. 05 to 08 with time.

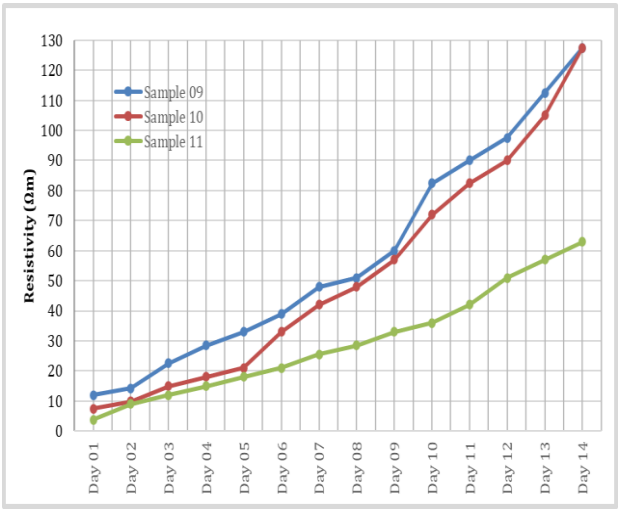

Fig. 4. Resistivity variation of sample No. 09 to 11 with time.

According to Fig. 4, Sample 11 is the best one among others. Sample 11 was also compared with Sample 06 and Sample 07; the resistivity values of Sample 11 was less than all others. Hence, Sample No. 11 has been selected as the best composition among all of the other samples considered in these experiments.

Sample 11, the percentage of the Cement, Sand, Metal, Bentonite, and Fly Ash are 20 %, 20 %, 40 %, 7.5 %, and 12.5 %, respectively, as given in Table VI. Finally, another two 150 × 150 × 150-mm^3 test cubes (without using aluminum plates) were molded for compression strength testing. After 7 days first test cube was crushed from the Compression strength testing machine. The result of the compressive strength of the sample was 1.68 N/mm^2 and the specimen density of the sample was 1947.9 kg/m^3. In a general rule, the concrete achieves 65% of their full strength after 7 days; following the same, the calculated full strength was 2.58 N/mm^2. Accordingly, the forecasted 7 days strength was poor. Therefore, a second test cube was crushed after 28 days. The Compressive strength value was 3.89N/mm^2 and the Specimen density value was 1998.8 kg/m^3. Twenty-eight-day compression strength is almost 100 % strength which was also poor. This sample contained 20 % of Bentonite, Fly Ash mix, and 80% of Grade 30 concrete mix. The Grade 30 concrete approximate compression strength value is 30.0 N/mm^2, but 20% of Bentonite and Fly ash mix has decreased the strength from 30.0 N/mm^2 to 3.89 N/mm^2.

Bentonite and Fly Ash mixed samples are given low resistivity values during the first two weeks. Afterward, resistivity values of Sample No. 11 were gradually increased to a higher level but the resistivity value of Sample 04 was in

TABLE VI. COMPARISON OF COMPOSITION OF SAMPLE NO. 09 TO 12

Ingredient	Sample			
	09	10	11	12
Cement	20%	20%	20%	22.50%
Sand	20%	20%	20%	22.50%
Metal	40%	40%	40%	45%
Bentonite	2.50%	5%	7.50%	3.75%
Fly Ash	17.50%	15%	12.50%	6.25%
Coir	0%	0%	0%	0%

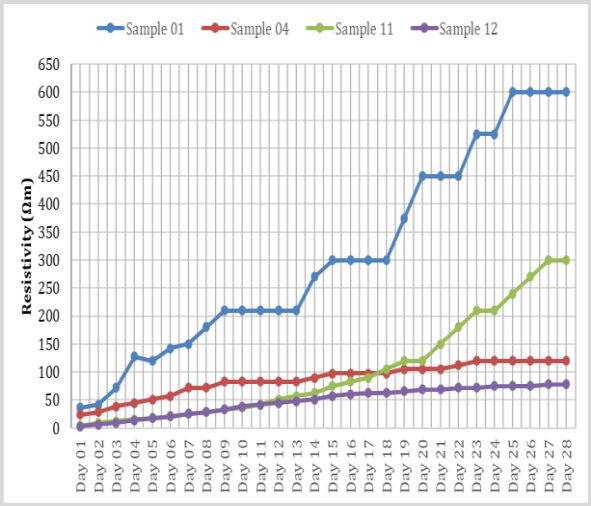

Fig. 5. Resistivity variation of sample No. 11 and 12 with time.

steady level as shown in Fig. 5. Gradually reducing the water content of Sample 11 was the reason for this. But the water retention capability of Sample 04 was at a high level. It means Bentonite has a good water absorption level and low water retention level. In concrete, the initial stage was not good but it was kept a steady level after that.

Sample 11 is the mixture of 80 % of concrete and 20 % of Bentonite and Fly Ash, Sample 12 is the mixture of 90 % of concrete and 10 % of Bentonite and Fly Ash as per Table VI. According to Fig 5, we can observe that Sample 12 gives low resistivity value during the first two weeks and it became steady at the rest of the time. It means it has a good water absorption level as well as a good water retention level. Bentonite is the reason for having a good water absorption level and concrete is the reason for having a good water retention level.

Fly Ash acts as good conductive and electrolytic material. Seven-day compression strength test was done for Sample No. 12 and it gave a specimen density of 2251.8 kg/m^3 and compressive strength of 16.5 N/mm^2. When converting that 65% of compressive strength value to their full-strength value, it becomes 25.35 N/mm^2.

Fig. 6. Variable frequency testing.

TABLE VII. CURRENT VARIATION WITH VOLTAGE AND FREQUENCY

AC Voltage	Current (mA)		
	50Hz	100Hz	150Hz
50	84	80	85
100	172	170	187
150	267	270	287
200	362	370	387
250	461	475	494
300	562	585	605

It is seen that the currents through the sample test cubes are increased with the frequency at the same voltage as given in Table VII. It can be assumed that the AC impedance of the material is gradually reduced with the frequency. The test apparatus used in the variable frequency test is shown in Fig.6. Finally, Sample No. 12 has been selected as the best composition for the backfill material.

C. Most Effective Dimension of Earth Pit

It says 94 % of the grounding resistance of a given electrode is determined by the character of the native soil within the Interfacing Hemisphere. Hence it is obvious that replacing the soil with a more conductive soil could achieve the desired objective. However, that action may prove impractical. A more practical action may be to replace only the part of the soil that exercises the greatest influence on the ultimate grounding resistance and to use the lowest resistivity soil available. Fig. 7 demonstrates the influence of the surrounding soil as a function of the radius of what is called the critical cylinder (that is, the soil immediately around the grounding electrode). According to Fig. 7, 52 % of the connection to earth is completed by a 0.3-m diameter critical cylinder, and 68 % of that connection is completed by a 0.6-m diameter critical cylinder. The most productive option is, therefore, expected to be between these two diameters.

It is seen that replacing soil in the interfacing hemisphere will reduce the resistance of the grounding rod to a certain extent. Since the maximum productive diameter of the backfilling critical cylinder is 0.6 m.

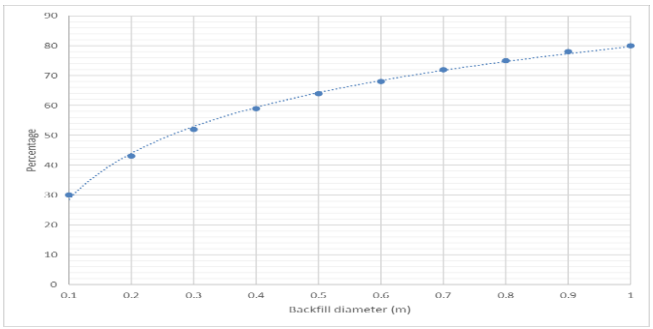

Fig. 7. Effectiveness of backfill diameter.

TABLE VIII. IMPROVEMENT WITH PARALLEL RODS

Diameter	Percentage of Resistance Improvement with no. of Parallel Electrodes (%)				
	1	2	3	4	5
0	0	42.4	56.5	64.7	70
0.1	31.85	60.75	70.35	75.94	79.55
0.2	44.31	67.92	75.77	80.34	83.29
0.3	51.6	72.12	78.94	82.91	85.48
0.4	56.77	75.1	81.19	84.74	87.03
0.5	60.78	77.41	82.94	86.16	88.23
0.6	64.05	79.29	84.36	87.31	89.22
0.7	66.82	80.89	85.57	88.29	90.05
0.8	69.23	82.27	86.61	89.14	90.77
0.9	71.34	83.49	87.53	89.88	91.4
1	73.24	84.58	88.36	90.55	91.97

D. Most Effective Earth Pit Dimension and Number of Parallel Electrodes

Experimentally it was seen 86.7% of distribution substation locations of a random sample of 30, native soil resistivity was increased with the depth. Hence longer rods will not give a considerable improvement of grounding resistance. It would be better to use parallel rods instead of increase rod height. Percentage of improvement of the earth resistance of the grounding system considering the resistivity of Sample No. 12 as backfilling material and with earth pit diameter is given in Table VIII.

IV. CONCLUSION

It was found that damages are recorded in the distribution network due to lightening. Although surge protective devices are used for the protection against lightning it was identified that some attention is required to locate surge protective devices effectively. Furthermore, it was identified that the full protection of the surge arrestors is not given due to the inductive impedance of the grounding system during impulse conditions. Hence, it is recommended to consider ac impedance rather than dc resistance of the earth terminals of surge arrestors since Sri Lanka is located relatively high lightning prone area considering the other countries in the world.

A. Usage of Backfill Material

Conductive concrete is used worldwide to enhance soil resistivity. Conductive concrete is a cementitious and carbonaceous material. It speeds up and improves the performance of earthing. Further, conductive concrete absorbs moisture from the surrounding soil and hardens to become part of the grounding electrode. The surface area of the electrode is thus dramatically increased and resistance to ground is substantially reduced.

CEB uses a cylindrical concrete block of 0.3 m radius and for the height of the earth rod for the soils having resistivity less than 200 Ωm [4]. However, the composition of the concrete mixture has not been well defined in manuals. A quality checking system for the concrete mixture for grounding is currently not available. Hence, the best concrete composition for better performance of earthing has been investigated. Accordingly, it has been noticed that the resistivity of the compound increases with the cement composition, and grade 30 concrete has the best performances.

Clay-based backfill materials such as Bentonite are used for improving ground resistance, but they are highly variable with respect to moisture. Carbon-based backfill materials such as Charcoal and Fly Ash can also be used to enhance soil resistivity. They are electrolytic and have water-retention capability inferior to clays. Usage of Coir to enhance grounding resistance has also examined. It has been found that there is no positive effect of adding Coir to the backfill mixture.

Since grade 30 concrete is the best composition for low resistivity, it was decided to add clay-based material and carbon-based material for enhancing the effectiveness. Bentonite and Fly ash are selected evaluating performances, cost, difficulty of usage, and availability.

The effectiveness has compared by measuring the resistance of standard test molds. Resistivity was calculated by using respective resistance values and the dimension of the test mold. However, the performances of adding Bentonite and Fly ash were evaluated while optimizing the cost too. Meanwhile, most effective backfilling volumes while varying the pit dimension and number of parallel earth pits were also examined.

Concrete is a well-known and freely available compound all over the country. Bentonite and Fly ash are also common materials and the mixing method is also simple. However, it is needed to measure soil resistivity and calculate the earth resistivity value of vertically driven earth rod (without backfill) firstly. Afterward, it is needed to calculate the percentage of resistivity improvement, select the cost-effective diameter of backfilling material, and the number of parallel electrodes by using elaborated in Table VIII. Finally, it was decided that the composition of Sample No. 12 is the most cost-effective with the performances as a backfill agent for SPD grounding.

The earth resistance for lightning surges increases in comparison with its resistance to static conditions. Thus, increasing the length of the earth electrode over the critical length will not cause a massive reduction of earth impendence to transients. Although earth rods are commercially available from 1.2 m up to 3 m, it is recommended to use 1.2-m rods for the grounding terminal in Sri Lanka.

While analyzing the recorded past lightning damaged incidents in the field, it is recommended to continue the shortest possible length of 50-mm^2 or grater copper earth cable. However, to reduce the inductive effect, a cable contained hair conductor strands will give better results while maximizing the skin effect.

B. Further Study

It is recommended to further study on transient analysis of the improved backfilled grounding system at lightning conditions. This could be done in computer software simulation in MATLAB. At lightning impulse, currents have high magnitudes in the range up to a few hundreds of kA. The rise time of the lightning impale is very short in the range of microseconds (μs). Thus, the typical lightning strike reaches a few hundreds of kA/μs. The current density of the soil near the earth rod becomes a very high value. As a result of that, the electric field strength increases up to values that cause

electrical dischargers in small gaseous voids in the soil resulting in ionization of soil around earth electrode, decreasing the ground resistivity and earth resistance. This phenomenon occurs mainly near-earth electrode. The intensity of this phenomenon is very high when the soil is dry or high resistive. The inductance of the metal parts of the earth electrode is usually neglected when considering earth impedance at network frequency of 50Hz. However, the inductance becomes an important parameter when the current flow rate is high in the range of kA/µs. During Lightning strikes inductive voltage drop, L (di/dt) reaches very high value and it leads to a reduction in the flow of surge current to the earth mass.

It would be better to check these samples at an HV lab while applying a lightning impulse to examine lightning impulse current characteristics and maximum voltage that appears between the ends of the protector due to its impedance as surge current pass through. It is recommended to simulate the proposed grounding system during a lightning impulse condition in ANSYS Maxwell or suitable simulation software to ensure the backfill composition and dimensions.

ACKNOWLEDGMENT

The authors express sincere gratitude to Mr. M.R. Ranathunga, Additional General Manager (Projects), and Mr. H.K. Illeperuma, Project Director (Green Power Dev. & EEIP-Tranch II) of Ceylon Electricity Board for supervising this research project. Also, we thank Mr. K.G.R.F. Comester, Deputy General Manager (Research & Development), Ceylon Electricity Board for facilitating the research throughout the period.

Authors would also like to thank Dr. M. N. Susantha Perera, Additional General Manager (Transmission), Ceylon Electricity Board for all strength provided to drive this project towards success.

REFERENCES

[1] J. He, R. Zeng, and B. Zhang, METHODOLOGY AND TECHNOLOGY FOR POWER SYSTEM GROUNDING 2013. Department of Electrical Engineering, Tsinghua University, China.

[2] S- C. Lim, C. Gomes, and M. Z. A. Ab Kadir, Characterizing of Bentonite with Chemical, Physical and Electrical Perspectives for Improvement of Electrical Grounding Systems. Centre for Electromagnetic and Lightning Protection Research (CELP): Department of Electrical & Electronics Engineering, University Putra Malaysia.

[3] IEEE Std 80-2000, (Revision of IEEE Std 80-1986), IEEE Guide for Safety in AC Substation Grounding. Sponsor Substations Committee of the IEEE Power Engineering Society Approved 30 January 2000.

[4] Ceylon Electricity Board, “Guideline for Distribution System Earthing (Part 1)”, 1998

Study and Implementation of Diesel Generator Soundproofing

Isanka Ehelepola
Workshop and Ancillary Services
Ceylon Electricity Board
Colombo, Sri Lanka
isankae@gmail.com

***Abstract*— This paper provides an in-depth study into the acoustic design of enclosures for diesel generator (DG) soundproofing. The enclosure has been mathematically modeled and the model is optimized using the Genetic Algorithm (GA) and Particle Swarm Optimization (PSO) for soundproof enhancement. The comparison of optimization results has shown that PSO provides a global optimum solution with less computational complexity. Theoretical derivation of enclosure dimensions for 100 kVA generator and minimized cost has been found by PSO for sound pressure level (SPL) objective of 65 dBA at a 3-m distance. The measurements carried out with the fabricated enclosure has shown good agreement with theoretical calculations. Further enhancement of the enclosure with sound absorption material has shown commendable SPLs related to soundproofing throughout the band of octave frequencies.**

Keywords—Diesel generator, enclosure, genetic algorithms, particle swarm optimization, soundproofing

I. INTRODUCTION

Installation of a diesel generator (DG) as a standby power supply is becoming an essential part to secure uninterrupted power in building service engineering as well as other social service activities. The operation of DG sets should be soundproof as it generates noises vibrating its structures as well as air. The structural vibration is controlled by using vibration isolators and/or dampers. Enclosures and silencers are widely used cost-effective methods of Passive Noise Controlling which attenuate the airborne noise emanated by introducing sound barriers consisting of sound-absorbing materials.

Commonly used commercially available standby DG sets are in the ratings of 10 kVA to 1250 kVA. Open type DGs within that power ratings generate overall noise starts from 90 dB(A) to 110 dB(A) a distance 1-m hearing point depending on make and model [1]. In Sri Lanka, Central Environment Authority has defined noise ordinance for the installation of noise-generating machinery to which an individual or the public is exposed. As per the Act, the maximum permitted overall noise level at the property line ranges from 45 dB(A) to 75 dB(A) depending on the location and Zone [2]. Hence the level of sound emission to the surrounding area is an important design concern when installing a DG set.

Predicting the performance of an acoustic enclosure is a challenging task. The empirical model proposed by Jackson in which the sound source and enclosure were modeled as infinite parallel plates is one of the first attempts to predict the performance of an acoustic enclosure [3]. Jugner has improved Jackson's Theory by modeling the enclosure as a finite rectangular piston source [4]. Jugner's model is also not compelling because it assumes an unrealistic source of vibration. In 1991, Oldham and Hilerby have developed a Mathematical model to predict IL of close-fitting enclosure considering vibration of enclosure panel caused by acoustic pressure generated by sound source [5,6]. This mathematical model reflects the relationship of material properties, thickness, and source to panel distance of the enclosure. According to the validation of Blank [7], Oldham and Hilerby's theory closely follows the actual behavior of the close-fitting enclosure. Based on the theory of Oldham and Hilerby, a mathematical model has been developed to predict the Sound Pressure Level (SPL) of DG Enclosure in [8]. An optimized design parameter for the fabrication of the DG enclosure for an open DG of standby power rating of 22 kVA has been found in [8] using the Genetic Algorithm (GA) method. Further, it has been validated by fabricating an enclosure for the open DG.

Commercially available soundproof standby DGs capacity below 500 kVA are fabricated as standard packaged units and the DGs above 500 kVA are fabricated as power box type. The size and the sound pressure level (SPL) of those standard products are fixed which gives limitations at the point of installations especially in limited spaces covered by a lot of obstructions. As a solution DG supplier imports open DGs and do the soundproofing locally to suit the space available. Though it is designed and manufactured in a compact product, making a product complying with required SPL is failed in most cases. A survey on this problem revealed that enclosure fabrication is done by considering the space available only and the generator soundproofing is done just by adding sound insulation material and silencers based on experience and one to one copying of imported products. Also, in Sri Lanka, acoustical designers are very less and there is no stipulated design method for acoustical enclosure design which is different from architectural acoustics.

II. METHODOLOGY

In industrial applications, the sound is measured from Sound Pressure Level (SPL) at a selected distance from the sound source. The performance of an acoustic enclosure is measured by Insertion Loss (IL) which is the SPL difference of a machine at a point outside the enclosure before and after the installation of the enclosure. As such performance of enclosure defines the SPL of the final product and it has to be designed based on the SPL of machinery to be soundproof without enclosure.

In order to calculate IL of the enclosure design for DG, the mathematical model developed in [8] was used. Insertion Loss of a Panel (IL_{Panel}) use for the fabrication of enclosure has mathematically modeled by (1),

$$IL_{Panel} = 10\log_{10}\left[\left(\cos(kd) + \left(\frac{\pi^2}{4K\omega\rho_0 c}\right)\sin(kd)\right)\right]^2 \quad (1)$$

where,

$$k = \frac{1.35}{\left[3.86D\left(\frac{129.6}{a^4} + \frac{78.4}{a^2b^2} + \frac{129.6}{b^4}\right) - \omega^2\rho h\right]} \quad (2)$$

$$D = \frac{Eh^3}{12(1-\nu^2)} \quad (3)$$

k - Acoustic wave number, $= \frac{2\pi f}{c}$
d – Source to panel distance in m
f -Frequency of the sound wave in Hz
ρ_0-Density air ($406\ kg/m^3$)
c - Speed of sound in air ($343\ m/s$)
D –Bulk Modulus of panel
a – Length of the panel in m
b – Width of the Panel in m
h – Thickness of the Panel in m
E – Panel's' Young modulus N/m^2
ν – Poison Ratio of the Panel Material
ρ- Density of Panel Material kg/m^3

Using (1), a mathematical model for IL of the enclosure was developed with the following assumptions.

- The sound source (Open DG) is a cuboid placed on a non-reflective surface and five sides are vibrating panels.
- Enclosure panel exposed to a uniform pressure field over the frequency spectrum.
- Noise contribution through the structure-borne path is negligible.
- 1:1 mode of the structure is the only effective radiator of sound.
- The enclosure is fabricated with five nos. of sheet metal panel (five faces of the cuboid excluding the base plate).

Total SPL after introducing a soundproof panel is calculated as total SPL of octave band frequency (SPLTF) which can be calculated by (4),

$$SPL_{TF} = 10\log_{10}\left[\sum_{i=1}^{11} 10^{\frac{(SPL_i - IL_i)}{10}}\right] \quad (4)$$

where, i is octave band frequency index (16, 32, 64,125,250,500,1k, 2k, 4k, 8k,16k), SPL_i is SPL of open DG at the i^{th} frequency, IL_i is IL of the panel at i^{th} frequency.

Sound Pressure Level of DG (SPLEDG) after covering the open DG by five sides is given by (5),

$$SPL_{EDG} = 10\log_{10}\left[\left(\sum_{i=1}^{5}\left(10^{\frac{SPL_{TF}}{10}}\right)\right)\Big/5\right] \quad (5)$$

where i is panel number (1 to 5).

The objective of the introduction of an enclosure to a DG is the reduction of SPL. Hence (3) is taken as the objective function for the minimization of SPL_{EDG} up to the required level. The objective function is developed by (1) & (4). As per (1) it is clear that by changing the enclosure material (ρ, E & ν), enclosure material thickness (h), and distance between sound source and panel (d), SPL_{EDG} can be changed. The following selections and boundaries have been considered for some of the design variables.

- Fixed the enclosure panel material as Galvanized Steel which is the cost-effective generally used material.
- Sheet metal thickness (h) is fixed as 1 mm – 3 mm considering the market availability and capability of fabrication.
- Source to panel distance (d) is fixed as 0.1 m -1 m under the concept of the close-fitting enclosure.

Optimization of value for h and d to achieve the required SPL level at minimum cost has to be done. The selection of the most suitable optimization method to solve the problem was aimed at numbers of variables, linear or nonlinear behaviors of the mathematical model, and numbers of constraints. In this problem, there are four design variables (i.e., sheet metal thickness (h), source to panel distance from length side (d1), width side (d2), and topside (d3)). The mathematical model represents nonlinear behavior and there is a cost constrain function.

In [8], a methodology to address this problem using the Genetic Algorithm (GA) has been proposed. The Genetic Algorithm is a metaheuristic inspired by the processes of natural selection which belongs to larger class evolutionary algorithms. This is used to generate highly accurate solutions for optimization problems and it is relying on bio-inspired operators such as mutation, crossover, and selection.

In order to identify the best suitable optimization method for solving this problem another method called Particle Swarm Optimization (PSO) was considered. Particle Swarm Optimization is another heuristic optimization method which was inspired by the swarming or collaborative behavior of birds or fish [9, 10]. The algorithm is similar to GA in terms of evolutionary algorithms. In each iteration, PSO and GA move from a set of points (population) to another set of points in solution space which provides likely improvement. However, unlike GA, PSO has no evolution operators such as mutation, crossover, or selection which demands additional computational cost. In PSO, Potential solutions fly through the problem space by following the current optimum solutions. Hence POS is much more capable of exploration of solutions in the problem space [11].

Here in this project both GA and PSO methods were considered to determine an optimized solution and then the best one was selected based on the solutions obtained. Open type standby power DG with the capacity of 100 kVA was selected as the sound source. The length, width, and height of the DG are 2.15 m, 0.55 m, and 1.42 m, respectively. Sound Pressure Level measurements of the open generator have to be measured as input data for the mathematical model developed in (1), (4) & (5). Considering the nature of the sound source and testing space, the standard given under ISO 3744 was used for obtaining SPL reading at engineering-grade accuracy. As per the standard followings were taken for SPL measurements.

i. The sound measurement point was selected as a 3-m distance from the open DG.

TABLE I. SPL MEASUREMENTS

Frequency/ Hz	16	32	64	125	250	500	1k	2k	4k	8k	16k
SPL/ dB(A)	36	52	89	84	91	93	91	91	87	85	79

ii. The sound was measured at 8 locations by locating the microphone at the points defined under ISO 3744 and the Logarithmic average of SPL measurements at eight points shall be taken as overall SPL.

iii. SPL was measured over the octave band frequency spectrum by using VT RAT 168B Real-Time Audio Spectrum Analyzer and the readings given by analyzer were validated by measuring overall SPL using Testo 816 Sound Level Meter which was calibrated by Industrial Technology Institute. The measured SPL data are given in Table I.

The objective function was defined in such a way that SPL_EDG converges to range between 65 - 70 dB(A) while the enclosure cost is minimized. SPL_EDG value range of 65 - 70 dB(A) has defined as an average value given in Schedule IV of Regulation 7a of section 32 of National Environmental Act No. 47 of Sri Lanka [2]. Enclosure cost was calculated based on the market value of GI sheet metal panels. Equation (6) was used for calculating the enclosure material cost.

$$\text{Enclosure material cost} = \text{The surface area of enclosure} \times (2167 \times h \times 1000) \quad (6)$$

By using the equation cost constraint is defined at Rs. 130,000.00 for enclosure material. Boundary values of h, d1, d2, d3 were defined as follows based on the conditions mentioned in section 2.2.

i. $0.001\text{m} \leqslant h \leqslant 0.003\text{m}$; h is sheet metal thickness

ii. $0.1\text{m} \leqslant d1 \leqslant 1\text{m}$; d1 source to panel distance in length side

iii. $0.1\text{m} \leqslant d2 \leqslant 1\text{m}$; d2 source to panel distance in width side

iv. $0.1\text{m} \leqslant d3 \leqslant 1\text{m}$; d3 source to panel distance in the top side

Initially, the GA method was used for optimization, and then the same optimization was done using the PSO method. This optimization was done for achieving SPL_{EDG} value of 70 dB(A). A comparison between two optimization methods is given in Table II and these results were obtained after executing the algorithms 100 times each.

TABLE II. OPTIMUM VALUE FOR ENCLOSURE*

Parameter	Genetic Algorithm method	Particle Swarm Optimization method
h / m	0.001437	0.001398
d_1 / m	0.549853	0.549402
d_2 / m	0.476928	0.490424
d_3 / m	0.429504	0.463211
Enclosure Cost/ Rs	69,998.55	69,613.55
Average Execution Time /s	10.101	3.732

*SPL of 70 dBA at a 3-m distance.

TABLE III. OPTIMUM VALUE FOR ENCLOSURE

Parameter	Particle Swarm Optimization method
h / m	0.002289
d_1 / m	0.578485
d_2 / m	0.554260
d_3 / m	0.550109
Enclosure Cost/ Rs	124,247.19

The results given by two optimization methods show that the PSO method gives the global optimum solution compared to the GA method because the optimum values yielded by GA significantly differ once the program is executed repeatedly. Also, the PSO provided better results with less computational complexity (i.e., significantly faster) in the process of finding a global minimum of the enclosure design cost and it provided consistent results even after the execution of algorithm hundred times. Therefore, it can be assured that the results obtained by PSO give an optimum set of values of the parameter which corresponds to the global minimum of SPL at an acceptable level of accuracy.

After the above mentioned finding the optimization of this enclosure problem was further done by using PSO for achieving the SPL level of 65 dBA at a 3-m distance. Table III provides the results of further optimization.

It was further observed that the enclosure design cost increases as SPL_{EDG} decreases in the considered neighborhood ($65 \leq SPL_{EDG} \leq 70$). Minimum cost for $SPL_{EDG} = 70$ is the upper bound considered and the cost is Rs. 69,571.00 For the lower bound of $SPL_{EDG} = 65$ the minimum cost is Rs. 124,247.19. For the preferred range of SPL_{EDG} it was observed that there is a linear relationship between enclosure design cost and SPL_{EDG} which is illustrated in Fig. 1.

III. RESULTS AND ANALYSIS

The results obtained by PSO were validated by design and fabrication of enclosure for open DG with a standby power rating of 100 kVA. Dimensions of the enclosure designed and fabricated are given in Table IV while the prototype is shown in Fig. 2.

After the fabrication of the enclosure, the SPL measurements were taken by covering the open DG and the same procedure described above was followed. The measured values are given in Table V as a comparison of SPL after and before enclosed with the fabricated enclosure.

TABLE IV. DIMENSIONS OF THE DESIGN AND FABRICATION

Dimension	Designed Enclosure	Fabricated Enclosure
Length / mm	3232	3235
Width/ mm	1819	1830
Height / mm,	2048	2065
Metal Thickness / mm	2.289	2

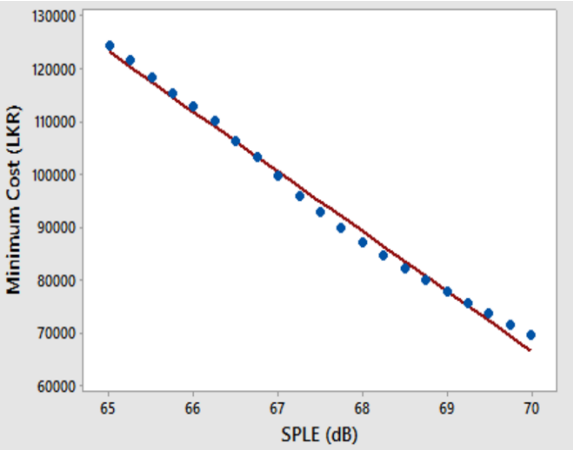

Fig. 1. Enclosure design cost vs SPL_{EDG}.

Fig. 2. Fabricated enclosure and sound pressure measurements.

TABLE V. COMPARISON OF MEASURED AND THEORETICAL SPL

Octave Band Freq. (Hz)	Sound Pressure Level (dB(A))		
	Measured Overall		Theoretical
	Enclosed	Open	Enclosed
16	23	34	49
32	43	50	39
63	68	87	63
125	73	83	49
250	76	86	53
500	78	91	48
1000	78	90	41
2000	79	90	32
4000	74	86	26
8000	74	84	18
16000	57	78	03
Overall	**85**	**97**	**64**

As per the data given in Table V overall SPL of the DG before enclose was 97 dBA at 3 m distance and it was reduced up to 85 dBA after putting the enclosure. However, the expected value of 65 dBA has achieved by the fabricated enclosure. The theoretical SPL calculated for dimensions of the fabricated enclosure are also given in Table V for comparison.

In theoretical calculation, the IL model was developed as a sealed box without any openings. But in actual implementation, it is compulsory to allow adequate openings in the enclosure for supplying fresh air for combustion and ventilation of the engine. The opening size at the inlet and outlet path is determined by referring to the air volume requirement given in the engine datasheets. In this case, openings with the dimension of 2'x 2'-4" were made at the wide side of the enclosure. Noise leaks though the enclosure is predominant, as well as the air, is flowing through the enclosed space at higher velocity affecting the reduction of Insertion Loss (IL) performance of the enclosure.

Suppression of SPL in each frequency is illustrated in Fig. 3. As per the figure, SPL within the frequency range 63 Hz to 8000 Hz is higher than 65 dB(A) which has to be reduced in order to achieve the required SPL. Also, it is clear SPL contribution of very low frequency is negligible. Under this circumstance, the IL performance of the enclosure can be further improved by introducing sound insulation material to the internal surface of the enclosure because sound insulation materials possess the property of absorbing the energy of high-frequency sound waves.

IV. FURTHER IMPROVEMENT

In this design concept enclosure was a closed-fitting type where the source panel distance is less than 1 m and the enclosure material is Galvanized steel with 2-mm (SWG 14) thickness. This is a rigid surface causing structural resonance due to panel vibration and cavity resonance within the narrow air gap. As a result, internal noise increased and allow more noise leaks through the enclosure. This can be reduced by insulating the internal surface of the enclosure for absorbing sound waves hit on the surface. Rockwool, Glass wool and foam materials are the readily available sound insulation material that can be used for Generator soundproofing applications. these materials are selected based on the factors that the amount of SPL to be reduced at different frequencies, cost, availability, density, flame retardant capability, resistance to abrasion and wear, aesthetic, ease of cleaning, health & safety, etc. By analyzing available materials in the market Polyurethane Foam Material (Procell) with the specification given in Table VI was selected for this application.

The internal surface area of the enclosures was insulated with the above-mentioned material and the SPL data with that enclosure was taken. As per the measurements, overall SPL has reduced up to 78 dBA from 85 dBA after introducing 2" thickness Polyurethane Foam Material to the enclosure. Even though this value can be improved further by adding another layer of the sound absorption material, the resultant effect is not significant. This has been clearly illustrated in [8]. Suppression of SPL in each frequency after the introduction of sound insulation material is illustrated in Fig. 4. As per the representation SPL at higher frequencies has reduced up to the expected level even tough SPL ant low frequencies are remaining high.

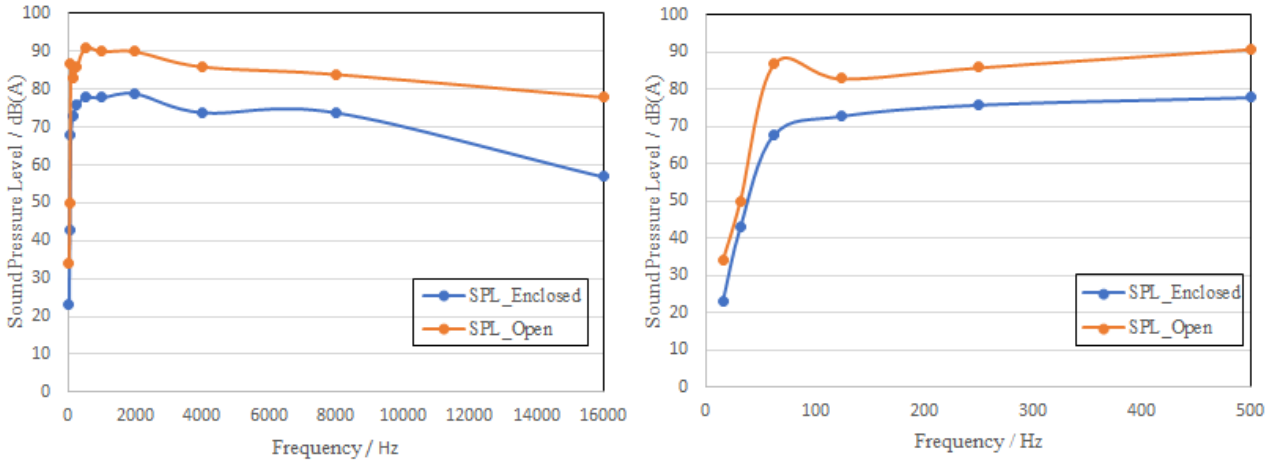

Fig. 3. SPL vs octave band frequencies.

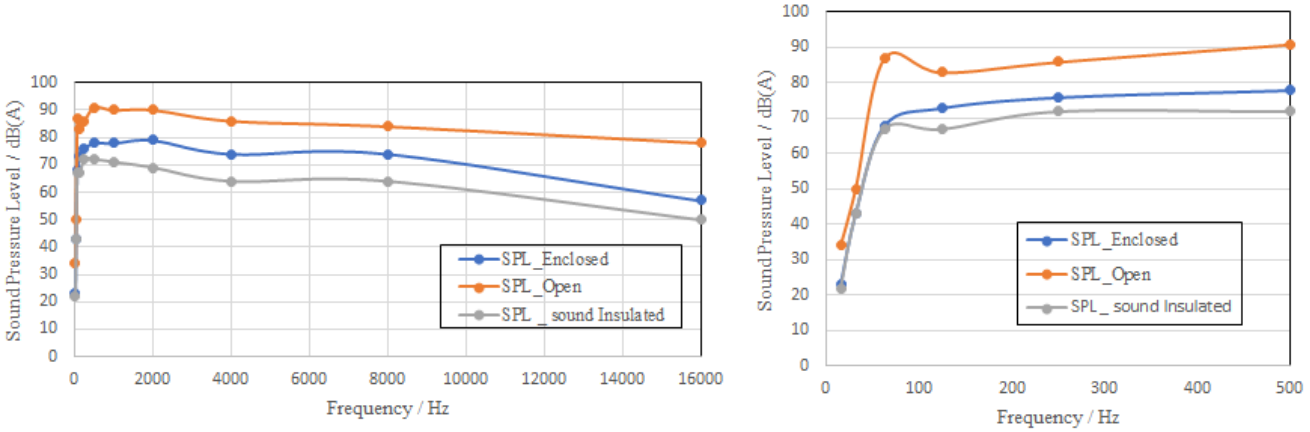

Fig. 4. SPL vs octave band frequencies after introducing sound absorption material.

V. Conclusion

The developed mathematical model for designing an enclosure for DG gives realistic values that were validated by SPL calculations and measurements of open DG. The study showed that PSO provided better results than GA with less computational complexity in the process of finding a global minimum of the enclosure design cost. Also, the values of the design parameter given by the algorithm were realistic and that can be used more accurately for enclosure fabrication. With the development of this optimization algorithm, it was enabled to introduce a more developed methodology for designing an enclosure for sound source by introducing SPL, cost, and space constraints.

Results obtained from the PSO method were validated by fabricating an enclosure for a DG with a standby rating of 100 kVA. Sound Pressure Level measurements were taken complying ISO3744 standard at maximum load of the DG. The overall SPL open DG was 97 dBA and the enclosed DG was 85 dBA at a 3-m distance. The expected SPL was 65 dBA which was not achieved by the enclosure. The main reason for the gap is allowing openings in the enclosure for providing ventilation and combustion air of the engine. The noise leaks trough openings are predominant and the percentage of noise leaks through the openings depend on the size and the orientation of the openings [12].

TABLE VI. Material Specifications

Specification Description	Product Data
Material type	Polyurethane Foam Material (Procell)
Density	70±5 kg/m³
Thickness	2mm
Thermal Conductivity	0.045 W/mk
Thermal Resistance	-30°C +130°C (Short Usage) / -30°C +100°C (Regular Usage)
Sound absorption value	Greater than 0.8 at higher frequencies.

Then the enclosure was further improved by introducing sound insulation material on the internal surface of the enclosure for reducing internal noise generated due to structural resonance and cavity resonance. By considering SPL values of different frequencies, a polyurethane foam material with the thickness of 2” was selected. This has reduced the overall SPL up to 78 dBA. The introduction of more insulation material is not a feasible solution compared to the material cost and the amount of SPL reduction.

In addition to noise leaks through the opening, the measured data can be affected by the noise of circulation air generated in the operation of the resistive load bank. The

background noise before starting the load bank and DG was 56 dBA and it was increased up to 63 dBA after starting the load bank at no load. This background noise also significantly affected noise data measurement.

The design variables obtained by the developed methodology can be used to do the preliminary design of a closed-fitting enclosure. With the preliminary design, the ultimate performance can be improved by introducing the sound attenuators to the inlet and exhaust openings. Finally, It proves that this study results opened a path to the local DG enclosure fabrication industry to do their design with a background of acoustic design rather than one to one mirror imaging of an existing enclosure.

The foremost investigation shall be focused on the noise leaks through the opening for air ventilation. Further acoustical study shall be carried through research to compensate for the reduction of the acoustic performance of enclosure through the openings. To date, most of the researches has focused on Passive Noise Controlling (PNC) for machine soundproofing. However, a hybrid noise controlling method can be investigated for controlling of SPL since the PNC works best for high-frequency pressure waves. The exhaust and inlet air noise of PG associated with low-frequency pressure waves which are unable to mitigate by PNC successfully. As a solution, the noise in ventilation air opening paths can be controlled by hybrid noise controlling. Initially, the air ventilation path can be designed with a duct that will provide passive noise control. Secondly, the uncontrolled low-frequency pressure waves can be controlled by introducing an Active Noise controller to the duct.

ACKNOWLEDGMENT

The author would like to express sincere gratitude to Mr. K. G. R. F. Comester, Deputy General Manager (Research & Development), Ceylon Electricity Board for providing the opportunity to carry out the study and for providing financial support with R & D funds. Also, the author would like to thank Mr. D. R. M. Harasgama, Deputy General Manager (Workshop & Ancillary Services), Ceylon Electricity Board for his valuable feedback as the supervisor of the study. Furthermore, the Author would like to thank the Supportive Committee members of the project; Mr. A.P.K. Muthunayake, Workshop and Ancillary Services, Mr. L.K. Fernando, Research and Development, and Mr. H.R.C. Amarsuriya, Workshop and Ancillary Services of Ceylon Electricity Board for their valuable support throughout the study.

Also, the author expresses gratitude for Mr. Manjula Pathiraja, Workshop and Ancillary Services, Ceylon Electricity Board, and the technical staff of Power Plant unit for giving their support for fabricating and testing of the enclosure.

Furthermore, the author extends sincere gratitude to Dr. U.K. Premaratne, Senior Lecturer, University of Moratuwa, and his Research Assistants Mr. K.A. Iroshan and Mr. A.D.N. De Zoysa for their intellectual support.

REFERENCES

[1] C.R. Krishna and J.E. Wegrzyn., "Survey on noise suppression system for engine generator sets", Research Development & Engineering survey report of Brookhaven National Library done by U.S. Army, October 1999.

[2] "The national environmental act, No 47 of 198", http://www.cea.lk/web/images/pdf/noise.pdf May 1996 [Sept. 4 , 2013].

[3] R.S. Jackson, "Some aspects of the performance of acoustic hoods," *Journal of Sound and Vibration*, vol. 3, no. 1, pp. 82 - 94, 1966.

[4] M.C Junger, "Sound transmission through an elastic enclosure acoustically coupled to a noise source," ASME Paper No. 70-WA/DE-12, 1970.

[5] D.J. Oldham and S.N. Hilerby, "The acoustic performance of small close fitting enclosures, part1 theoretical methods," *Journal of Sound and Vibration*, vol. 150, pp. 261 - 281, 1991.

[6] D.J. Oldham and S.N. Hilerby, "The acoustic performance of small closed fitting enclosures, part 2 Experimental & investigation," *Journal of Sound and Vibration*, vol.150, pp. 283 - 300, 1991.

[7] J.E Blank., "Optimal Design of an Enclosure for a Portable Generator," MSc Thesis, Virginia Polytechnic Institute and State University, Virginia, 1997.

[8] I. Ehelepola, and D.P. Chandima, "Design Optimization of Power Generator Soundproofing Enclosure Using Genetic Algorithm Tool," in *110th IESL Annual Session* 2016.

[9] J. Kennedy and R. Eberhart, "Particle swarm optimization," in *Proceedings of the IEEE International Conference on Neural Networks*, vol. 4, Piscataway, NJ, 27 November-1 December 1995, pp. 19421948.

[10] M. Clerc and J. Kennedy, "The particle swarm - explosion, stability, and convergence in a multidimensional complex space," *IEEE Transactions on Evolutionary Computation*, vol. 6, no. 1, pp. 5873, 2002.

[11] A. Ratnaweera, S. K. Halgamuge, and H. C. Watson, "Self-organizing hierarchical particle swarm optimizer with time-varying acceleration coefficients," *IEEE Transactions on Evolutionary Computation*, vol. 8, no. 3, pp. 240255, 2004.

[12] D. C. Byrne, "The Consequence of "Leaky" Enclosures," National Institute of Occupational Safety and Health, Pittsburgh, Pennsylvania.

Technical and Economic Performance of PV Plus Battery Storage Domestic Systems Installed under NAMA Project

P. L. S. Bhasura
Transmission Design and Environment
Ceylon Electricity Board
Colombo, Sri Lanka
bhasura.liyanage@ceb.lk

A. L. Deshapriya
Research and Development
Ceylon Electricity Board
Colombo, Sri Lanka
asanga.lankanath@ceb.lk

D. S. P. Edirisinghe
Planning and Development
Distribution Division 4
Ceylon Electricity Board
Colombo, Sri Lanka
ee1prcpd.dd4@ceb.lk

***Abstract*— Supplying of night peak in the Sri Lankan grid is very challenging due to the operation of high-cost power plants to cater to the night peak demand. As a pilot project funded by the united nations development fund (UNDP), the possibility of reducing the domestic night peak load was tested by installing 14 solar photovoltaic (PV) systems with battery storages. In this analysis, we illustrate the performance of the aforementioned hybrid systems in the context of electrical energy such as power flow within the system, battery utilization, dependency to the grid, energy balance of the system, etc. It also provides an economic comparison of the system with the utility's power generation methods. The study has revealed that 67 % of the load energy is met by solar energy and the battery. The combined peak and daily dependencies of the systems have promising values of 32.7 % and 35.8 %, respectively. The combined battery utilization is found to be 47 .2 %. The unit cost assessment has proved that solar PV plus battery hybrid systems are currently not good candidates to reduce the night peak if the objective is only to reduce the night peak, due to the availability of cheaper power solutions.**

Keywords*— battery, daily dependency, hybrid, peak dependency, solar PV

I. INTRODUCTION

Domestic Solar PV net-metering system with battery storage has been identified as one of the key initiatives in Demand Side Management (DSM) practices. In order to meet this objective, Sri Lanka Sustainable Energy Authority (SEA) in partnership with United Nations Development Program (UNDP) has taken the initiative to carry out the pilot project by installing around 14 systems in the green zones of Kurunegala & Kotte CEB areas. This pilot project was carried out under the Global Environment Funded (GEF) Project on "Nationally Appropriate Mitigation Actions (NAMA) in the Energy Generation and End-Use Sectors in Sri Lanka.

Selected solar panel capacities in the project were ranging from 500 W to 3 kW while battery capacities were ranging from 2.4 kWh to 9.6 kWh depending on the customer's energy usage. Both li-Ion and Pb-Acid batteries were installed. During the daytime, the domestic solar PV system converts solar energy to electricity and cater to domestic load requirements, and any excess energy is stored in the battery bank. If more energy is available, this energy will be exported to the national grid. The stored energy will be used during the evening peak hours (6.30 PM - 10.30 PM) and if the domestic demand is higher than system capacity or the battery has insufficient energy to cater to domestic load, the system draws electricity from the national grid. If there is a power failure or load shading in the national grid, the system caters to the domestic load requirement with islanding operation. Battery storage will not be allowed to be charged from the grid or feed the grid at any time of operation.

Research & Development Branch of Ceylon Electricity Board carried out this study on the above installed solar battery hybrid systems to analyze the technical performance of each system, to check the grid dependability (Daily dependability & night peak dependability) and the effect of the total system (when considered all 14 installations as one system) on the utility grid.

II. METHODOLOGY

The methodology which was carried out during the study is illustrated in Fig. 1.

A. System Description

Four different types of solar battery hybrid systems installed under the project could be identified as given in Table I. Different types of Inverters named hybrid, micro & normal grid inverter with retrofitting units were used. Most of the batteries used are either Li-Ion (with DOD of 90%-95%) or Sealed Maintenance Free (SMF) Deep cycle Pb- Acid type (with DOD of 50%). In addition, saltwater gel/Na-Ion battery type is used in one installation. Table II provides the details of battery & inverter types and the cost of installation of each of the aforementioned systems.

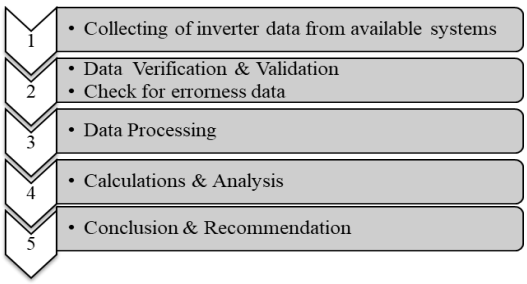

Fig. 1. Methodology

TABLE I. SYSTEM TYPES

System	Domestic Solar PV system capacity (W)	Battery Storage planned Capacity (kWh) at 80 % DOD
Type A	500	1.5
Type B	750	2.5
Type C	1250	4.0
Type D	3000	7.0

TABLE II. SYSTEM DESCRIPTION

	System Type & Capacity	Battery Capacity (Available) kWh	Battery Type (Li-Ion/ Deep Cycle Lead Acid SMF)	Installation Location	Inverter Type	Battery Origin	Total Price (LKR)
1	Type A/ 500W & 1.5kWh	2.4	Li-Ion	Kurunegala	Micro	Japan	960,000.00
2	Type B/ 750W & 2.5kWh	3.6	Li-Ion	Kurunegala	Micro	Japan	1,350,000.00
3	Type D/ 3000W & 7kWh	7.2	Li-Ion/Poly	Kotte	Hybrid	Korea	2,650,000.00
4	Type A/ 500W & 1.5kWh	2.34	SMF DC LA	Kurunegala	Hybrid	USA	700,000.00
5	Type B/ 750W & 2.5kWh	4.68	SMF DC LA	Kurunegala	Hybrid	USA	918,000.00
6	Type C/ 1250W & 4kWh	4.8	Li-Ion	Kurunegala	Hybrid	China	965,423.00
7	Type C/ 1250W & 4kWh	4.8	Li-Ion	Kotte	Normal grid inverter + Retrofitting unit	China	1,062,622.00
8	Type D/ 3000W & 7kWh	9.6	Li-Ion	Kotte	Hybrid	China	1,672,525.00
9	Type D/ 3000W & 7kWh	9.6	Li-Ion	Kurunegala	Normal grid inverter + Retrofitting unit	China	1,605,285.00
10	Type B/ 750W & 2.5kWh	5.76	SMF DC LA	Kurunegala	Normal grid inverter + Retrofitting unit	China	900,000.00
11	Type C/ 1250W & 4kWh	9.6	SMF DC LA	Kurunegala	Normal grid inverter + Retrofitting unit	China	975,000.00
12	Type C/ 1250W & 4kWh	5.2	SALT WATER GEL/Na-Ion	Kotte	Normal grid inverter + Retrofitting unit	USA	1,300,000.00
13	Type C/ 1250W & 4kWh	4.8	Li-Ion	Kurunegala	Hybrid	China	1,170,000.00
14	Type D/ 3000W & 7kWh	9.6	Li-Ion	Kurunegala	Hybrid	China	1,789,000.00

B. Operational Algorithm

The operational algorithm of the system was defined to cater to the night peak as much as possible from the battery and to fully utilize the solar energy. During the day time, the power generated by the PV module shall feed the domestic load first and then charge the batteries. Any excess power after charging the batteries shall be exported to the grid. If the generated power is not sufficient to meet the domestic load batteries should provide the balance requirement. When no power generation by PV in the night or due to overcast, batteries should provide the electrical load requirement. At any time if battery capacity is not adequate to meet the load, the grid should continue to provide power. The energy stored in the batteries should never be exported to the grid at any point of operation. The system should import energy from the grid if the load exceeds system rated capacity or does not have sufficient energy stored. However, batteries should not be charged by the grid electricity and batteries should not feed into the grid when the grid fails.

C. Data Processing

After filtering out the customers with unrealistic data, the remaining files were processed and used in the analysis. Further was observed that data from PV systems has been recorded for uneven time slots which could not be used for processing. Hence, the same data set has to be converted to

evenly processed data with the aid of a computer program. Python has been used to process the raw data and convert it to an analyzable format by averaging data to a 15-minute time interval.

D. Parameters for Technical Performance Analysis

The technical performance of each system was analyzed under the following derived parameters

Monthly Energy Balance: Monthly energy balance illustrates how the different sources of energy have been utilized by the customer for a given month which is represented by a bar chart.

Load Energy Balance: How the load energy (Energy consumed within the house) is catered is represented in this bar chart. There are three ways of serving the load namely, imported energy from the grid, discharged energy from the battery and the energy flows directly to the house due to solar PV generation

Solar Energy Balance: How the solar energy (generated by the PV system) is utilized is shown in this bar chart. Generated solar energy can be utilized to serve the domestic load during the day time, to charge the battery, or to export the excess energy (if any) to the national grid.

Daily Dependency: The ratio between the imported energy from the grid and the load energy that is consumed within the house for a particular month. This parameter describes the degree of dependency of each customer to the CEB grid.

Daily Dependency=(Imported Energy from the Grid for a given month (kWh))/(Load Energy consumed within the house in that month (kWh))

Peak Dependency: The ratio between the imported energy from the grid during the peak time (18:30hrs – 22:30hrs) and the load energy utilized by the consumer during the peak hours per a particular month is defined as the Peak Dependency. The dependability of each customer to the CEB grid during the peak time will be described by this parameter. Since one of the objectives of installing a solar battery hybrid system is to reduce the night peak of the load curve, having a low peak dependency will be benefited to the utility.

Peak Dependency=(Imported Energy from the Grid during the night peak for a given month (kWh))/(Load Energy consumed during the night peak within the house in the same month (kWh))

Battery Utilization: Up to which extent the battery is utilized is described by this parameter. Ideally, the battery should be charged fully and discharged fully for a particular day which means the battery utilization is 100%. However, in practice, the battery is not ideally utilized due to prevailing issues such as less solar generation due to rain, less load energy to cater, etc.

Battery Utilization=(Discharged Energy from the battery for a particular month (kWh))/(Battery capacity × Depth of Discharge of the battery×30)

Round Trip Efficiency of the storage: The ratio of the energy put into the storage and the energy retrieved from the storage is defined as the round trip efficiency of the storage system. Energy storages typically consume a part of electricity stored into that system (due to internal resistance etc.). Hence the discharged energy is always lesser than the stored energy.

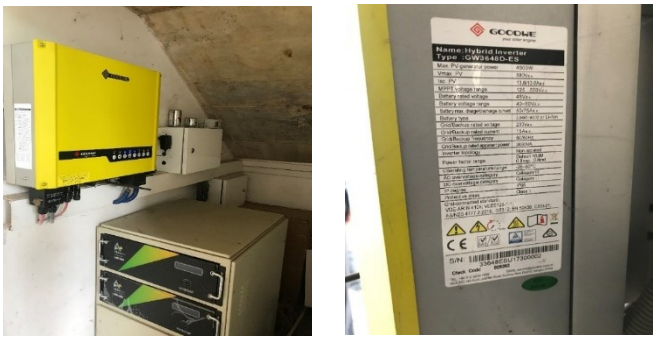

Fig. 2. System installation.

Round Trip Efficiency of the storage=(Discharged Energy from the battery for a particular month (kWh))/(Stored Energy to the battery for the same month (kWh))

III. Performance Analysis of a Selected System

The selected system depicted in Fig. 2 was owned by a customer in the Green Village, Kurunegala, and the installed capacity of Solar PV panels is 3 kW. The battery capacity is 7 kWh. The Solar PV plus battery hybrid system consists of twelve polycrystalline 260-W solar panels, two Li-ion batteries with a total capacity of 7 kWh and a hybrid inverter.

The "Average Power Profile" is shown in Fig. 3. According to it, the solar power generation starts around 6.00 a.m. It can be identified that the all most all the demand of the house has been provided by the direct solar power. The surplus solar power has been used to charge the batteries. When the SOC of the batteries is around 80% the charging rate of the batteries drops and the excess power exports to the utility grid. During the day time, the battery charges to its maximum. In the evening, the solar power generation falls and the load is served by discharging the battery and importing from the utility grid. According to Fig. 3, the stored energy in the batteries caters to the total overnight demand of the house. In the morning around 4.30 a.m., the load of the house increases, and a very small amount of energy has been imported from the utility grid to cater to the deficit between the load and the discharge of the battery.

Fig. 4 shows the load energy balance of the customer for each month. The load energy can be supplied from the imported energy from the utility grid, discharged energy from the battery, and from the solar energy which is directly fed to the customer load through the inverter. According to Fig. 4, the required energy to the load has been served from the battery discharged energy and direct solar energy. The import of energy from the utility grid is very small compared to the load energy requirement. In March, May, and October the import of energy is zero. This indicates the excellent performance of the system, which is fully independent of the utility grid in terms of energy. But with the available data, it cannot be declared that the house is fully independent of the utility grid in terms of power. Fig. 5 illustrates the solar energy balance. Solar energy balance shows how and to what extent solar energy has been utilized in the system. Solar energy from the PV panels feed the domestic load through the inverter and if there is excess energy it charges the battery and export to the utility grid. According to Fig. 5, it could be identified that a major portion of generated solar energy has been exported to the utility grid. Battery charging has not been performed as expected in March, May, and October. But in February, July, August, and September, a considerable amount of energy has

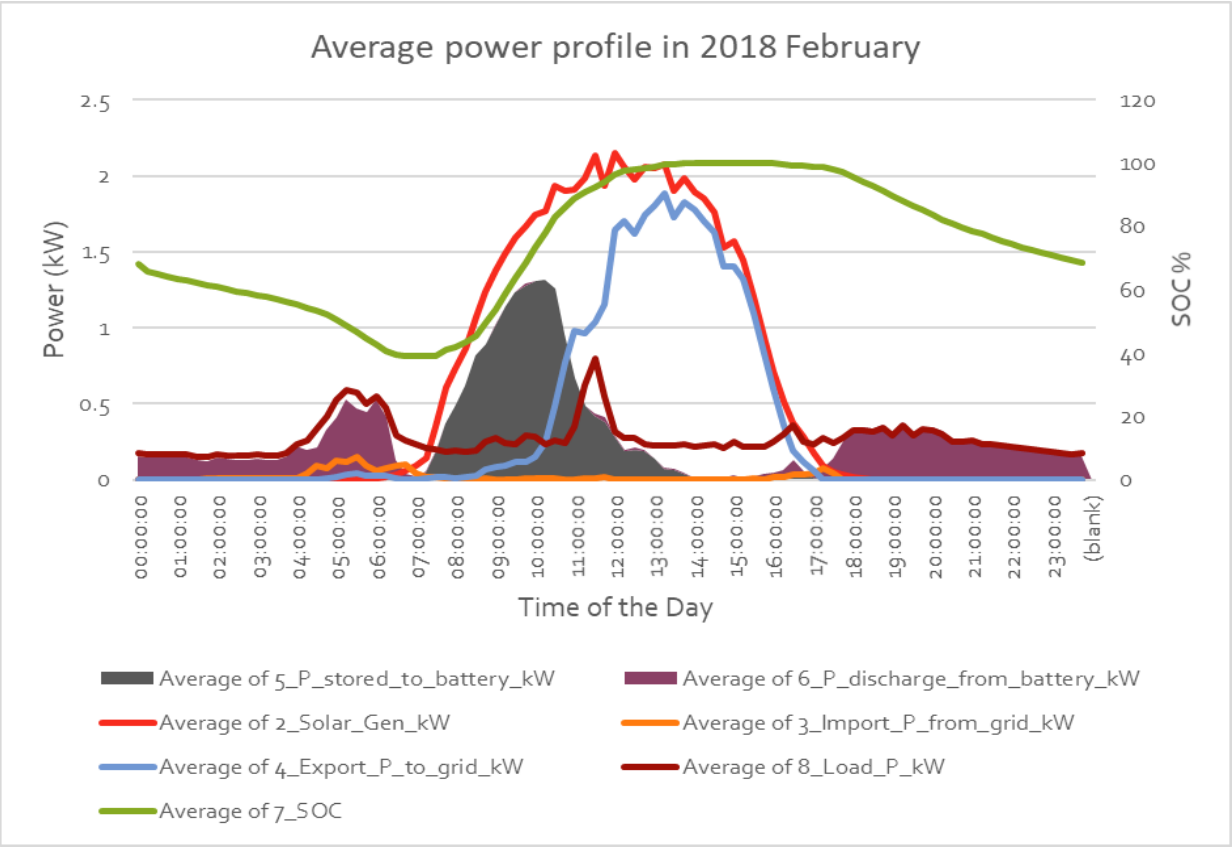

Fig. 3. The average power profile of February 2018.

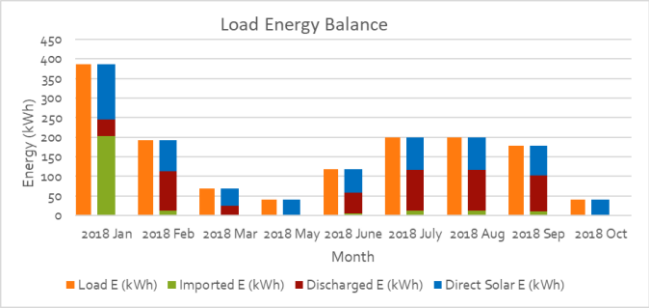

Fig. 4. Load energy balance.

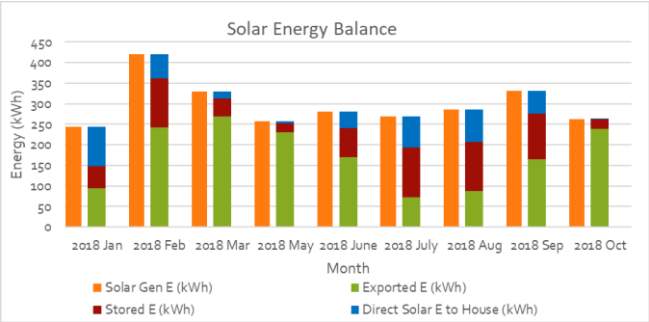

Fig. 5. Solar energy balance.

been stored in the battery. This could be misleading that the system is not performing well. But the reason for the low amount of discharging in March, May, and October is the smaller load energy demand in that period. There was no considerable load to discharge the stored energy in those months. The Solar PV system has generated 421 kWh in February which is the maximum and 244 kWh in January which is the minimum.

The Daily Dependency of the customer has been calculated for each month and plotted as in Fig. 6. According to Fig.6, the Daily Dependency in January is more than 50 % which the loads have imported from the utility grid. In the other months, the Daily Dependency is less than 10 %, which means only about 10 % of the energy requirement of the house has been catered from the utility grid. This indicates that the energy requirement of the house is less dependent on the utility grid. Excellent system performance has been achieved which leads to a higher level of independence from the utility grid.

The Peak Dependency of the customer has been calculated for each month and plotted as in Fig. 7. As per Fig. 7., in January, the Peak Dependency is about 75 %. This means that 75 % of the energy requirement of the house during peak hours has been imported from the utility grid. However, from February onwards, the Peak Dependency of the house is zero. This indicates the excellent performance of the system which was fully independent of the utility grid during peak hours.

The calculated Round Trip Efficiency of the battery has been shown in Fig.8. In May and October, the Round Trip Efficiency is zero which indicates that the battery discharge has not occurred. In March, Round Trip Efficiency is 53 %. In the other months, the Round Trip Efficiency of the battery is in the range of 75 % -100 % which could be considered as better performance. This indicates that more than 75 % of the energy stored in the battery is discharged to serve the loads of the house.

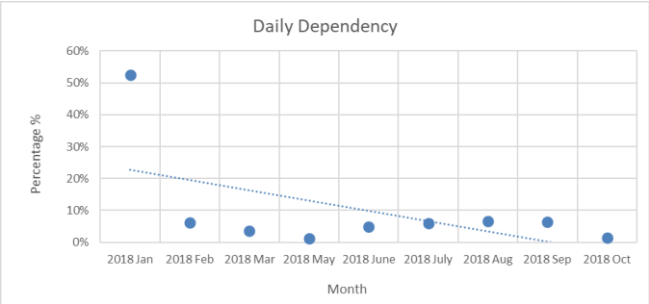

Fig. 6. Daily dependency.

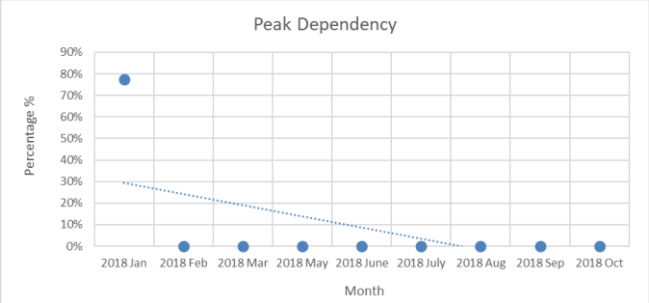

Fig. 7. Peak dependency.

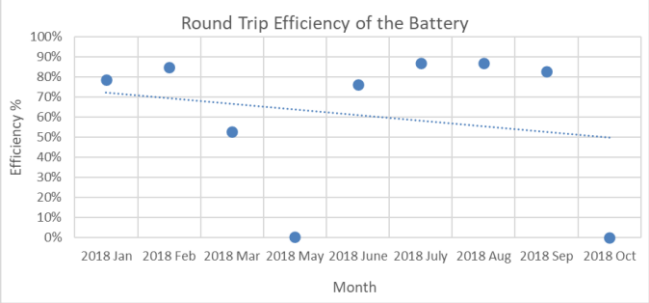

Fig. 8. Round trip efficiency of the battery.

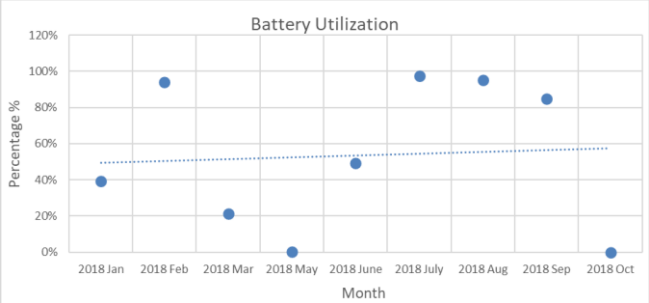

Fig. 9. Battery utilization.

The battery utilization shown in Fig. 9 indicates the performance of the battery relative to the capacity of the battery. According to Fig. 9, the battery utilization is not satisfactory. This is solely due to the lower energy demand of the customer. With this analysis, it can be concluded that the Solar PV plus battery hybrid system has been over-designed.

IV. Analysis of Combined Effect

Following the same methodology, six more customer systems were individually analyzed as in the previous section. Consequently, the "Yearly Average Power Profile" was developed by considering all seven customers. The total solar capacity of combined systems is 10.5 kW and the total battery capacity is 39.6 kWh. This graph shows the average yearly impact of the combined 7 system. Since there is no data for some months for customers, the yearly average power profile for each customer was developed by averaging the data of available months. Yearly average power profile shown in Fig. 10 was developed by taking the summation of yearly average load profiles of each customer.

Fig.10 demonstrates the variation of battery charging power, battery discharging power, solar generation, imported power from the grid, exported power from the grid, and the power consumed within the house. It can be observed that solar generation starts every day around 6 AM and since the solar generation is minimal, load demand supplies by importing the balance amount from the grid and discharging batteries. When the solar generation increases, the domestic electricity demand can be supplied from the grid and excess energy is used to charge the battery. If the summation of battery charging power and load power is less than the solar generation power then the excess solar generation has exported to the grid. The battery started to discharge around 4 PM when the solar generation is very small. In that time load power met by solar generation, battery discharging, and importing the power from the grid. Always power consumed line lies above the battery discharging power curve and imported power curve which means the total load was supplied by a combination of the battery discharging, importing from the grid, and the solar energy. The area during the night peak time provides the load energy supplied from the battery and the grid. Even though all systems have a solar plant with a total capacity of 10.5 kW, the maximum solar generation of the solar plant is around 6.5 kW. It is visible that around 67 % of the load energy met by solar energy and the battery. Key output parameters of combined analysis are given in Table III. Technical performance analysis parameters given in Table IV were calculated from the values given in Table III for May 2018.

TABLE III. Key Output Parameters

Monthly Average Solar generation (kWh)	1,231.33
Monthly Average Imported energy (kWh)	458.11
Monthly Average Exported energy (kWh)	399.65
Monthly Average Stored energy (kWh)	564.47
Monthly Average Discharged energy (kWh)	505.27
Monthly Average load energy (kWh)	1,278.12
Monthly average peak time imported energy (kWh)	87.69
Monthly average peak time load energy (kWh)	267.44

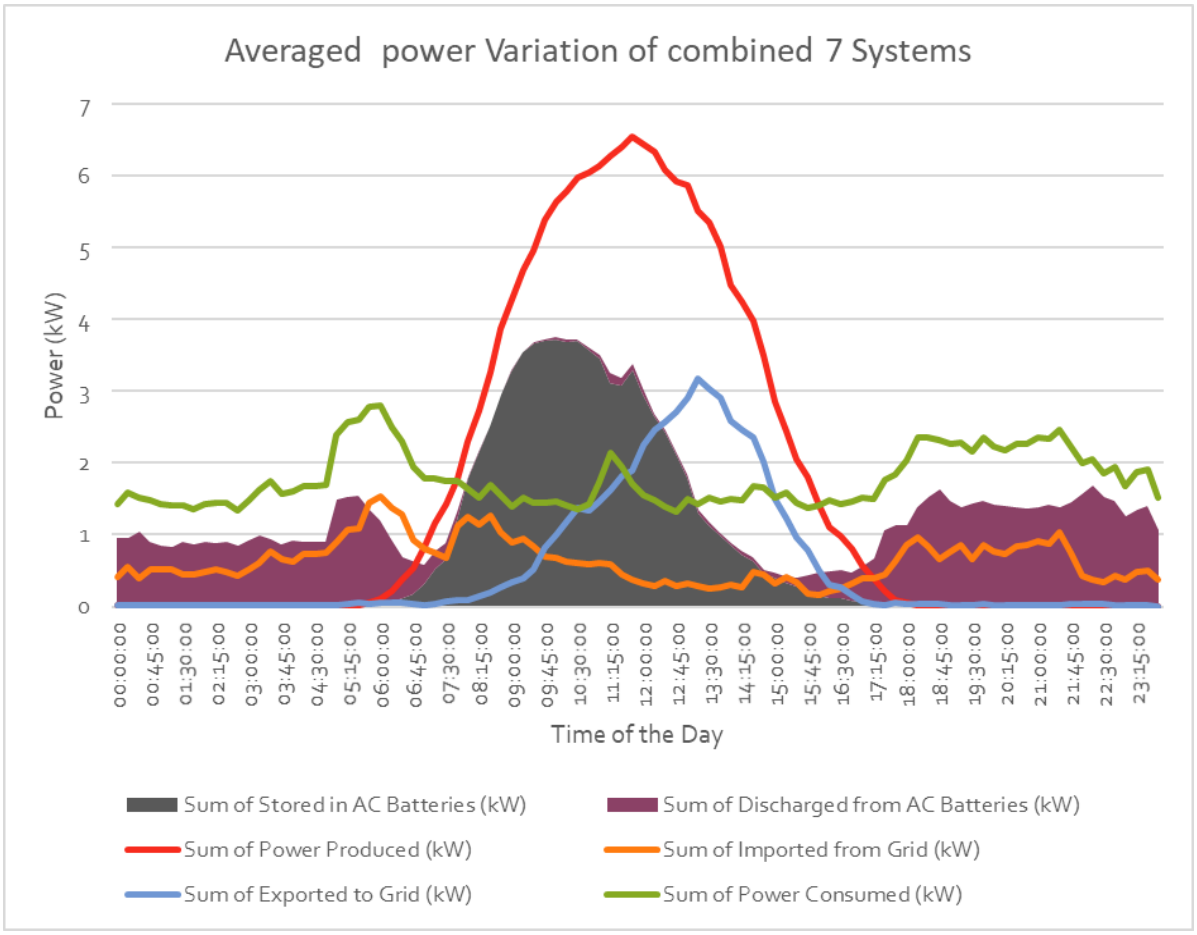

Fig. 10. Combined average power variation.

TABLE IV. TECHNICAL PERFORMANCE ANALYSIS PARAMETERS

Combined Battery utilization of 7 systems	47.2 %
Combined Peak dependency of 7 systems	32.7 %
Combined Daily dependency of 7 systems	35.8 %

Combined Peak dependency and daily dependency of 7 systems are 32.7 % and 35.8 %, respectively which is a good result. Battery utilization of the combined system is around 47.2 % which means that only half of the battery has used throughout the year. This is due to the insufficient solar capacity to charge the battery fully, incorrect programming of hybrid inverters for discharging, and whether conditions.

V. UNIT COST ASSESSMENT

The main objective of solar battery hybrid system is to reduce the night peak by storing solar energy to battery and use the stored energy in the peak time. In addition to that, the main advantage of CEB from such a project is reducing the night peak. In order to check the financial viability of a National level project of installing solar-battery hybrid systems by the utility to curtail the night peak, unit cost assessment was carried out. Unit cost figures were calculated under the following two scenarios:

1. With the only purpose of curtailing the night peak (using the battery discharge energy), which was otherwise be served by a high-cost power plant

2. Considering also the capacity savings due to serving the day time load demand by solar PV and the excess solar energy exported to national energy, in addition to the night peak reduction

Table V provides the installation costs of each system studied in previous sections assuming a 25-year lifetime. In unit cost comparison of peak discharged energy, it is assumed that total investment is made to reduce the night peak by discharging the stored energy in the battery. Costs of a peak unit otherwise served by the highest cost power plant were calculated for the systems of each customer and provided in Table VI.

TABLE V. SYSTEM INSTALLATION COST

Customer	Cost of the installation - LKR
Customer 1	1,789,000.00
Customer 2	1,170,000.00
Customer 3	1,062,622.00
Customer 4*	1,672,525.00
Customer 5	965,423.00
Customer 6	960,000.00
Customer 7	1,350,000.00

*analyzed in Section III.

TABLE VI. COST OF PEAK UNIT

Customer	Cost of a peak unit which otherwise served by the highest cost power plant – LKR/kWh
Customer 1	166.87
Customer 2	154.16
Customer 3	127.98
Customer 4	264.99
Customer 5	131.24
Customer 6	393.93
Customer 7	277.92
KPS Small GT*	45.12

*Kelanitissa power station small gas turbine.

TABLE VII. UNIT COST OF CUSTOMERS

Customer	Cost of a unit of the system – LKR/kWh
Customer 1	31.40
Customer 2	29.09
Customer 3	23.92
Customer 4	23.14
Customer 5	38.44

It can be concluded that solar plus battery storage systems are not a viable solution to reduce the night peak if the objective is only to reduce the night peak by looking at the values in Table VI.

Peak saving is not the only benefit that is gained by installing a solar battery hybrid system. The system can be used to serve the day time load demand of the house and also the export of any excess energy to the national grid which were otherwise served by a power plant. Hence, the capacity of the power plant (e.g., Storage level of a hydro plant) can be saved to cater to the peak instead of dispatching it during day time.

Table VII provides, the unit costs of customers who installed solar battery hybrid systems when considering the battery discharging during the peak time, day time load-serving by direct solar energy and exporting excess energy to the national grid. The cost values vary from 23.14 LKR/kWh to 38.44 LKR/kWh which is in the range of unit cost paid for solar under private power purchase agreement (PPA) of CEB.

VI. CONCLUSION AND RECOMMENDATIONS

In this paper, the performance of solar PV plus battery hybrid systems of 7 customers in the UNDP NAMA project has been studied to investigate the possibility of reducing the domestic night peak load to the utility. It was found that 67 % of the load energy is met by solar energy and the battery. The combined peak and daily dependencies of the systems were promising with values of 32.7 % and 35.8 %, respectively. The combined battery utilization was found to be 47 .2 % which has considerable capacity in enhancement with proper sizing and installation of the systems.

The unit cost assessment has proved that solar PV plus battery hybrid systems are currently not good candidates to reduce the night peak if the objective is only to reduce the night peak, due to the availability of cheaper power solutions.

It is recommended to administer careful installation and commissioning procedures to avoid reduced system performance from the beginning due to incorrect configurations (e.g., added limitation to battery power during the peak time, import energy stored to the battery due to the incorrect programming of the hybrid inverter) and also to cater for low customer knowledge and technical capacity concerning solar PV plus battery hybrid systems. It is also necessary to check the log files of the hybrid inverter or retrofitting unit which contains important electrical parameters of the system after one month of operation. Furthermore, the Sri Lankan grid experiencing a rapid decrease in demand just after the night peak. Therefore, it is better not to utilize batteries in the system after the night peak.

ACKNOWLEDGMENT

The authors would like to thank the officers of Sustainable Energy Authority, Sri Lanka, and UNDP NAMA Project for their coordination and support provided throughout the study in terms of the provision of information, data, and access to the systems.

Research & Development Branch

CEB , 2 nd Floor,Block No. 5, BMICH, Bauddhaloka Mawatha, Colombo 7

Tel. : 011 269 7033 / Fax : 011 269 7022 /e-mail : dgmrd@ceb.lk / web : www.ceb.lk